

Phenomenology of a Higgs triplet model at future e^+e^- colliders

Sylvain Blunier,^{1,*} Giovanna Cottin,^{2,†} Marco A. Díaz,^{1,‡} and Benjamin Koch^{1,§}

¹*Instituto de Física, Pontificia Universidad Católica de Chile, Av. Vicuña Mackenna 4860, Santiago, Chile*

²*Cavendish Laboratory, University of Cambridge, J.J. Thomson Ave, Cambridge CB3 0HE, UK*

(Dated: April 11, 2017)

In this work, we investigate the prospects of future e^+e^- colliders in testing a Higgs triplet model with a scalar triplet and a scalar singlet under $SU(2)$. The parameters of the model are fixed so that the lightest CP -even state corresponds to the Higgs particle observed at the LHC at around 125 GeV. This study investigates if the second heaviest CP -even, the heaviest CP -odd and the singly charged states can be observed at existing and future colliders by computing their accessible production and decay channels. In general, the LHC is not well equipped to produce a Higgs boson which is not mainly doublet-like, so we turn our focus to lepton colliders. We find distinctive features of this model in cases when the second heaviest CP -even Higgs is triplet-like, singlet-like or a mixture. These features could distinguish the model from other scenarios at future e^+e^- colliders.

I. INTRODUCTION

The discovery of the Higgs boson at the LHC [1, 2] confirms the particle content of the Standard Model (SM) of particle physics. Still one of the main beyond the SM puzzles remains neutrino mass generation. Several extensions to the SM Higgs sector that give a mass term to neutrinos involve the spontaneous violation of lepton number via the vacuum expectation value of an $SU(2)$ singlet (for a review, see Ref. [3]). A common feature of these models is the presence of a massless goldstone boson, the Majoron J .

We investigate the phenomenology of a Higgs triplet model (HTM) of the kind mentioned above that has a scalar singlet and a scalar triplet under $SU(2)$, in addition to a $SU(2)$ scalar doublet. The model was originally proposed in [4], where the authors defined it as the “123” HTM. Once the triplet field acquires a vacuum expectation value (vev), a neutrino mass term is generated. The parameters in the neutrino sector include the vev of the triplet and the Yukawa couplings between the two-component fermion $SU(2)$ doublet, including charged leptons and majorana neutrinos, and the triplet field. In this work, we study the collider phenomenology of the “123” model, which is almost decoupled from its neutrino sector [5]. This is why we don’t discuss experimental constraints on neutrino masses and mixing angles, which are beyond the scope of this paper and which we leave for a future work. Models in which neutrino masses arise from the interaction with a triplet field have also been discussed extensively in the literature [6–10].

The phenomenology of “123” models was studied before in [11, 12], paying particular attention to the consistency of the presence of the Majoron with experimental

data. The Majoron is mainly singlet in this model, so its interaction with gauge bosons such as the Z is negligible, making its existence fully consistent with collider data. This is in contrast to what happens in models with spontaneous violation of lepton number without the singlet field [13], which are excluded.

A characteristic signature of models with Higgs triplets is the existence of a doubly charged scalar ($\Delta^{\pm\pm}$), in addition to the existence of a tree-level $H^\pm W^\mp Z$ vertex, where H^\pm is a singly charged Higgs [7]. The LHC collider phenomenology of a doubly charged scalar in Higgs triplet models (in particular the “23” HTM, without the singlet field) has been discussed in [8, 14]. Production of doubly charged scalars at e^+e^- colliders has also been studied in the literature as probes of Higgs triplet models [15], the Georgi–Machacek model [16] and left-right symmetric models [17], which have a similar phenomenology.

The phenomenology of the neutral scalar sector in Higgs triplet models has been less studied than the charged sector. Production and decays of the neutral Higgs bosons in the “23” HTM, was studied in [18, 19]. Associated production of the charged and neutral Higgs at the ILC was studied in [20, 21]. In particular for the “123” HTM of interest in this paper, only discovery prospects at colliders were discussed in [11] and a fermiophobic Higgs was studied in [12].

The collider phenomenology of neutral and singly charged Higgs bosons in the HTM has received much less attention in the literature than the doubly charged Higgs. In addition, the phenomenology of the doubly charged Higgs depends directly on neutrino physics we are not evaluating at this time (as noticed earlier), so we focus on the neutral sector and singly charged Higgs of the “123” HTM.

In this paper, we study the production and decay of the next to heaviest neutral CP -even Higgs h_2 , the CP -odd Higgs A and the singly charged Higgs H^\pm of the “123” HTM. We extend the work in Refs. [11, 12] by identifying the lightest state in the CP -even neutral sector, h_1 , as the SM-like Higgs discovered at the LHC. This rules out the fermiophobic SM-like Higgs boson sce-

* sblunier@uc.cl

† gfc24@cam.ac.uk

‡ mad@susy.fis.puc.cl

§ bkoch@fis.puc.cl

nario described in [11]. Constrains are imposed on the parameter space of the model in order to retain the SM-like Higgs properties. In particular, we define h_1 to be mainly doublet and fix its mass to be $m_{h_1} \approx 125$ GeV. We also identify the necessary constrains on the parameters of the scalar potential to suppress its decays to Majorons, so that its invisible decay width is negligible.

We identify three characteristic benchmarks of the model related to the composition of h_2 . h_2 can be mainly singlet, mainly triplet or a mixture. Note that h_2 can not be mainly a doublet since this is reserved for the SM like Higgs-boson. We compute production cross-sections and decays in these three benchmarks. We find that the main 2-body production mode for h_2 is associated production with a CP -odd state A and note that cross-sections are in general larger when A is produced on-shell. Production of A may be observable at CLIC when produced in association with an h_2 or h_3 (the heaviest CP -even Higgs), depending on the benchmark. The singly charged Higgs boson H^+ is potentially observable at CLIC when produced in association with another H^- . Decay rates of h_2 to fermions are suppressed. Invisible decays of h_2 to Majorons can be very important, depending on the benchmark. Decays of $A \rightarrow h_i Z$, with $i = 1, 2$ or $A \rightarrow t\bar{t}$ dominate, depending on the benchmark. The decays of $H^\pm \rightarrow h_1 W^\pm$ dominate in all three benchmarks.

The paper is organized as follows. In Section II we introduce the model under study. Section III describes our restrictions and scan over the parameter space. In Section IV we comment on the low production cross-section of the new heavy Higgs of this model at the LHC. Section V describes production of h_2 , A and H^\pm at future e^+e^- colliders, while in Section VI we comment on the decay phenomenology of the model. We briefly comment on the most promising channels for discovery in Section VII. After a summary and conclusions in Section VIII we define the relevant Feynman rules in Appendix B, for easy reference by the reader.

II. THE MODEL

The model under consideration was introduced in Ref. [4] and studied further in Refs. [11, 12]. The scalar sector includes a singlet σ with lepton number $L_\sigma = 2$ and hypercharge $Y_\sigma = 0$, a doublet ϕ with lepton number $L_\phi = 0$ and hypercharge $Y_\phi = -1$, and a triplet Δ with lepton number $L_\Delta = -2$ and hypercharge $Y_\Delta = 2$. The notation we use is,

$$\begin{aligned}\sigma &= \frac{1}{\sqrt{2}}(v_\sigma + \chi_\sigma + i\varphi_\sigma), \\ \phi &= \begin{pmatrix} \frac{1}{\sqrt{2}}(v_\phi + \chi_\phi + i\varphi_\phi) \\ \phi^- \end{pmatrix}, \\ \Delta &= \begin{pmatrix} \frac{1}{\sqrt{2}}(v_\Delta + \chi_\Delta + i\varphi_\Delta) & \Delta^+/\sqrt{2} \\ \Delta^+/\sqrt{2} & \Delta^{++} \end{pmatrix},\end{aligned}\quad (1)$$

where $v_\sigma, v_\phi, v_\Delta$ are the vacuum expectation values (vev) of the neutral components of each scalar field. The presence of the triplet allows to have a term that can give mass to neutrinos [6, 7, 10].

Following the notation of [11], the scalar potential can be written as

$$\begin{aligned}V(\sigma, \phi, \Delta) &= \mu_1^2 \sigma^\dagger \sigma + \mu_2^2 \phi^\dagger \phi + \mu_3^2 \text{Tr}(\Delta^\dagger \Delta) + \lambda_1 (\phi^\dagger \phi)^2 \\ &+ \lambda_2 [\text{Tr}(\Delta^\dagger \Delta)]^2 + \lambda_3 (\phi^\dagger \phi) \text{Tr}(\Delta^\dagger \Delta) \\ &+ \lambda_4 \text{Tr}(\Delta^\dagger \Delta \Delta^\dagger \Delta) + \lambda_5 (\phi^\dagger \Delta^\dagger \Delta \phi) + \beta_1 (\sigma^\dagger \sigma)^2 \\ &+ \beta_2 (\phi^\dagger \phi) (\sigma^\dagger \sigma) + \beta_3 \text{Tr}(\Delta^\dagger \Delta) (\sigma^\dagger \sigma) \\ &- \kappa (\phi^T \Delta \phi \sigma + \text{h.c.}).\end{aligned}\quad (2)$$

Imposing the tadpole equations (the equations stating that the vev's are obtained at the minimum of the scalar potential) permits the elimination of the parameters μ_1^2 , μ_2^2 , and μ_3^2 in favor of the vev's [11].

When expanding around those vev's, the real neutral fields $\chi_\sigma, \chi_\phi, \chi_\Delta$ become massive. At the level of the Lagrangian this means that a term $\frac{1}{2}[\chi_\sigma \chi_\phi \chi_\Delta] M_\chi^2 [\chi_\sigma \chi_\phi \chi_\Delta]^T$ appears, where

$$M_\chi^2 = \begin{bmatrix} 2\beta_1 v_\sigma^2 + \frac{1}{2}\kappa v_\phi^2 \frac{v_\Delta}{v_\sigma} & \beta_2 v_\phi v_\sigma - \kappa v_\phi v_\Delta & \beta_3 v_\Delta v_\sigma - \frac{1}{2}\kappa v_\phi^2 \\ \beta_2 v_\phi v_\sigma - \kappa v_\phi v_\Delta & 2\lambda_1 v_\phi^2 & (\lambda_3 + \lambda_5) v_\phi v_\Delta - \kappa v_\phi v_\sigma \\ \beta_3 v_\Delta v_\sigma - \frac{1}{2}\kappa v_\phi^2 & (\lambda_3 + \lambda_5) v_\phi v_\Delta - \kappa v_\phi v_\sigma & 2(\lambda_2 + \lambda_4) v_\Delta^2 + \frac{1}{2}\kappa v_\phi^2 \frac{v_\sigma}{v_\Delta} \end{bmatrix}.\quad (3)$$

By diagonalizing this matrix with $O_\chi M_\chi^2 O_\chi^T = \text{diag}(m_{h_1}^2, m_{h_2}^2, m_{h_3}^2)$, one obtains the masses of the neutral scalar fields h_1, h_2 , and h_3 . The fields are such that $O_\chi [\chi_\sigma, \chi_\phi, \chi_\Delta]^T = [h_1, h_2, h_3]^T$. We assume that the lightest of them is the Higgs boson discovered in 2012 [1, 2], with mass $m_{h_1} \approx 125$ GeV [22]. In the present article we concentrate on the phenomenology of the second CP -even Higgs boson h_2 , the massive CP -odd Higgs

boson A , and the charged Higgs boson H^\pm , in consistency with the SM-like higgs found at the LHC being h_1 in the ‘‘123’’ model.

The pseudoscalar fields $\varphi_\sigma, \varphi_\phi$, and φ_Δ mix due to the mass matrix M_φ^2 . The term in the Lagrangian has the

form $\frac{1}{2}[\varphi_\sigma \varphi_\phi \varphi_\Delta]M_\varphi^2[\varphi_\sigma \varphi_\phi \varphi_\Delta]^T$ with

$$M_\varphi^2 = \begin{bmatrix} \frac{1}{2}\kappa v_\phi^2 \frac{v_\Delta}{v_\sigma} & \kappa v_\phi v_\Delta & \frac{1}{2}\kappa v_\phi^2 \\ \kappa v_\phi v_\Delta & 2\kappa v_\Delta v_\sigma & \kappa v_\phi v_\sigma \\ \frac{1}{2}\kappa v_\phi^2 & \kappa v_\phi v_\sigma & \frac{1}{2}\kappa v_\phi^2 \frac{v_\sigma}{v_\Delta} \end{bmatrix}. \quad (4)$$

By inspection, we know that there are two null eigenvalues, since two rows are linearly dependent of the third. The mass matrix is diagonalized by another rotation given by $O_\varphi M_\varphi^2 O_\varphi^T = \text{diag}(m_{G^0}^2, m_J^2, m_A^2)$, where G^0 is the massless nonphysical neutral Goldstone boson and J is the massless physical Majoron. A is the massive pseudoscalar, and $O_\varphi[\varphi_\sigma, \varphi_\phi, \varphi_\Delta]^T = [G^0, J, A]^T$ is satisfied.

The pseudoscalar A has a mass,

$$m_A^2 = \frac{1}{2}\kappa \left(\frac{v_\sigma v_\phi^2}{v_\Delta} + \frac{v_\Delta v_\phi^2}{v_\sigma} + 4v_\sigma v_\Delta \right). \quad (5)$$

A value of κ different from zero is necessary to have a massive pseudoscalar A . For experimental reasons, we would like to take the massless Majoron as mainly singlet in order to comply with the well measured Z boson invisible width [23, 24]. Nevertheless, in the “123” model imposing this is unnecessary because the Majoron results mostly singlet as long as the triplet vev is small (see Appendix A). The Majoron can acquire a small mass via different possible mechanisms [25]. In cases where this particle has a small mass, it can be a candidate for Dark Matter [26].

We mention also the electrically charged scalars. The singly charged bosons ϕ^{*-} and Δ^+ mix to form the term in the Lagrangian $[\phi^-, \Delta^{+*}]M_+^2[\phi^{*-}, \Delta^+]^T$, with

$$M_+^2 = \begin{bmatrix} -\frac{1}{2}\lambda_5 v_\Delta^2 + \kappa v_\Delta v_\sigma & \frac{1}{2\sqrt{2}}\lambda_5 v_\Delta v_\phi - \frac{1}{\sqrt{2}}\kappa v_\phi v_\sigma \\ \frac{1}{2\sqrt{2}}\lambda_5 v_\Delta v_\phi - \frac{1}{\sqrt{2}}\kappa v_\phi v_\sigma & -\frac{1}{4}\lambda_5 v_\phi^2 + \frac{1}{2}\kappa v_\phi^2 v_\sigma / v_\Delta \end{bmatrix}, \quad (6)$$

which is diagonalized by a rotation given by $O_+ M_+^2 O_+^T = \text{diag}(m_{G^+}^2, m_{H^+}^2)$. As in the previous case, by inspection this mass matrix has a null eigenvalue corresponding to the charged Goldstone boson. The mass eigenstate fields satisfy $O_+[\phi^{*-}, \Delta^+]^T = [G^+, H^+]^T$. The charged Higgs mass is,

$$m_{H^\pm}^2 = \frac{1}{2} \left(\kappa \frac{v_\sigma}{v_\Delta} - \frac{1}{2}\lambda_5 \right) (v_\phi^2 + 2v_\Delta^2). \quad (7)$$

Finally, the doubly charged boson Δ^{++} mass is given by

$$m_{\Delta^{++}}^2 = -\lambda_4 v_\Delta^2 - \frac{1}{2}\lambda_5 v_\phi^2 + \frac{1}{2}\kappa v_\phi^2 \frac{v_\sigma}{v_\Delta}. \quad (8)$$

since it does not mix (it is purely triplet).

III. RESTRICTIONS ON THE PARAMETER SPACE

In this Section we explain our restrictions on the model parameters. We first comment that the invisible decay width of the Z gauge boson in our model is suppressed since the Majoron J is mostly singlet ($O_\varphi^{21} \approx 1$). We define Γ_{inv}^{123} as the decay width of the Z into undetected particles excluding the decay into neutrinos, $Z \rightarrow \bar{\nu}\nu$. Experimentally, $\Gamma_{inv}^{123} < 2$ MeV at 95% CL. [23, 24] and in our model there could be a contribution from the mode $Z \rightarrow JZ^* \rightarrow J\bar{\nu}\nu$. This contribution is automatically suppressed because the Majoron is mainly singlet (see Appendix A).

Also, this model includes three CP -even Higgs bosons. We assume that the lightest of them is SM-like, and therefore fits with the experimental results. That is, we assume its mass is near 125 GeV, that it is mainly doublet ($O_\chi^{12} \approx 1$), and that its invisible decay width is negligible [27]. This last condition is obtained if we suppress the h_1 coupling to Majorons taking $|\beta_2| \leq 0.05$. The constraints we implement are:

- $|O_\varphi^{21}| \geq 0.95$ (J mainly singlet)
- The ρ parameter is also very well measured: $\rho = 1.00037 \pm 0.00023$ [23]. In this model it is

$$\rho = 1 - \frac{2v_\Delta^2}{v_\phi^2 + 4v_\Delta^2}. \quad (9)$$

This restricts the value of v_Δ to be smaller than a few GeV. Nevertheless, we consider $v_\Delta < 0.35$ GeV as in Ref. [11] in order to satisfy astrophysics bounds.

- $m_{h_1} = 125.09 \pm 0.24$ GeV [22].
- $|O_\chi^{12}| \geq 0.95$ (h_1 mainly doublet)
- $|\beta_2| \leq 0.05$ (small h_1 invisible decay)
- $m_{H^\pm} > 80$ GeV [23].

We make a general scan where we vary all the independent parameters. We generate their values randomly from uniform distributions. We do our scan with positive values of λ_1, β_1 and κ , as negative values of these

parameters typically result in negative eigenvalues of the mass matrix in eq. (3). The window for v_2 is reduced because of its dependency with the masses of the W and Z bosons [12]. Considering the range of v_2 and v_3 , the scanned range for λ_1 is mostly fixed due to its strong dependency with $m_{h_1} \approx 125$ GeV, and also because of the small effects of the mixings with other CP -even scalars (see eq. (3)). Terms outside of the mass matrix diagonal are generally much smaller than those on the diagonal, making the terms in the diagonal leading almost directly to the masses of h_1 , h_2 and h_3 . The scanned range for β_2 is forced to be small to avoid a large h_1 invisible decay (see Section VIA).

After imposing our constraints we note a clear hierarchy where $v_\sigma \gg v_\phi \gg v_\Delta$ that we have partially imposed: v_Δ is small in order to account for the measured ρ parameter, and $v_\phi \approx 246$ GeV to account for the Higgs mass. With that, a large value for v_σ comes naturally.

We find a small effect from our filters in λ_2 , λ_3 , λ_4 , λ_5 and β_3 . We note that the value of κ cannot be zero because in that case the CP -odd Higgs A would be massless, and since it is mostly triplet that would contradict the measurements for the invisible decay of the Z boson. Its value cannot be too large neither because mixing in the CP -even sector would move h_1 away from the mostly doublet-like scenario (a SM-like Higgs boson). After the scan and imposing the filters we can see the distribution of the physical masses in our model. This is shown in Fig. 1, where the thick black line shows the distribution before cuts to appreciate their effect. The most distinctive feature is that we impose the lightest scalar mass to be $m_{h_1} \approx 125$ GeV. All the other masses are free. The model allows for heavier scalars considering that we still have room for large parameters.

We highlight that the Majoron is massless in this model and is naturally mainly singlet, as can be inferred from eq. (A5), which is related to the exact diagonalization of the CP -odd mass matrix shown in Appendix A. Also notice that the new scalar states have the tendency to be heavy, with extreme values for the masses obtained for high values of the parameters. The shape of the distributions in Fig. (1) of course depends on using a linear generation of random values, which highlights large masses. Anyhow, we consider this to be an argument against colliders with small values for the centre of mass (CM) energy.

There is also an ambiguity related to the composition of the h_2 field: it can be mainly singlet, mainly triplet, or anything in between, as long as it is not mainly doublet, which is reserved for h_1 , our SM-like Higgs boson. If h_2 is mainly triplet its mass tends to be similar to the masses of A , H^+ , and Δ^{++} (all these fields are mainly triplet). If h_2 is mainly singlet, the mass of h_3 tends to be equal to the masses of A , H^+ , and Δ^{++} , and in this case, a mainly-singlet h_2 can be lighter. The masses of h_2 and h_3 are strongly correlated with the values of $(M_\chi)_{11}^2$ and $(M_\chi)_{33}^2$ depending on which is mainly singlet or triplet. Obtaining a scenario where h_2 and h_3 are not

purely singlet or triplet requires $(M_\chi)_{11}^2$ numerically very close to $(M_\chi)_{33}^2$, making that scenario highly fine-tuned.

The splitting between the mainly triplet fields is controlled by $|\lambda_5|$. This can be algebraically understood starting from the hierarchy $v_\Delta \ll v_\phi, v_\sigma$ and approximating eq. (5):

$$m_A^2 \approx \frac{1}{2} \kappa \frac{v_\sigma v_\phi^2}{v_\Delta} \quad (10)$$

Using the same approximation in eqs. (7) and (8), we get for the singly and doubly charged Higgs masses,

$$\begin{aligned} m_{H^\pm}^2 &\approx m_A^2 - \frac{1}{4} \lambda_5 v_\phi^2 \\ m_{++}^2 &\approx m_A^2 - \frac{1}{2} \lambda_5 v_\phi^2 \approx m_{H^\pm}^2 - \frac{1}{4} \lambda_5 v_\phi^2. \end{aligned} \quad (11)$$

Thus, H^\pm , Δ^{++} and A can differ appreciably in mass as long as $|\lambda_5|$ is large.

The previous considerations motivate us to define three benchmarks, characterized by the composition of h_2 in Table I. The parameters for each benchmark are defined in Table II. Note that these are chosen thinking of e^+e^- colliders, given the masses below 1 TeV.

We stress the fact that there is an ambiguity in the composition of h_2 . By definition h_1 is mainly doublet. The H^+ and Δ^{++} fields are always mainly triplet. The A field is also always mainly triplet because J is mainly singlet. The composition of h_3 is complementary to the composition of h_2 .

Table III shows the physical masses obtained for the three benchmarks. In B1 h_2 is mainly triplet, thus it has a mass similar to A , H^\pm , and Δ^{++} masses, with h_3 heavier. In B2 h_2 is mainly singlet, thus it is h_3 that has a mass similar to the masses of A , H^\pm , and Δ^{++} , with h_2 lighter.

IV. PRODUCTION AT THE LHC

Here we briefly comment on the production cross-section at the LHC for the scalars h_2, A and H^\pm for our model benchmarks (which we choose thinking of e^+e^- colliders). We implement the ‘‘123’’ HTM in FEYNRULES [28] and interface the output to the MADGRAPH5 [29] event generator to compute production cross-sections.

When thinking of a SM-like Higgs boson (such as h_1 in our model), the main production mode at the LHC is gluon-gluon fusion (ggF),

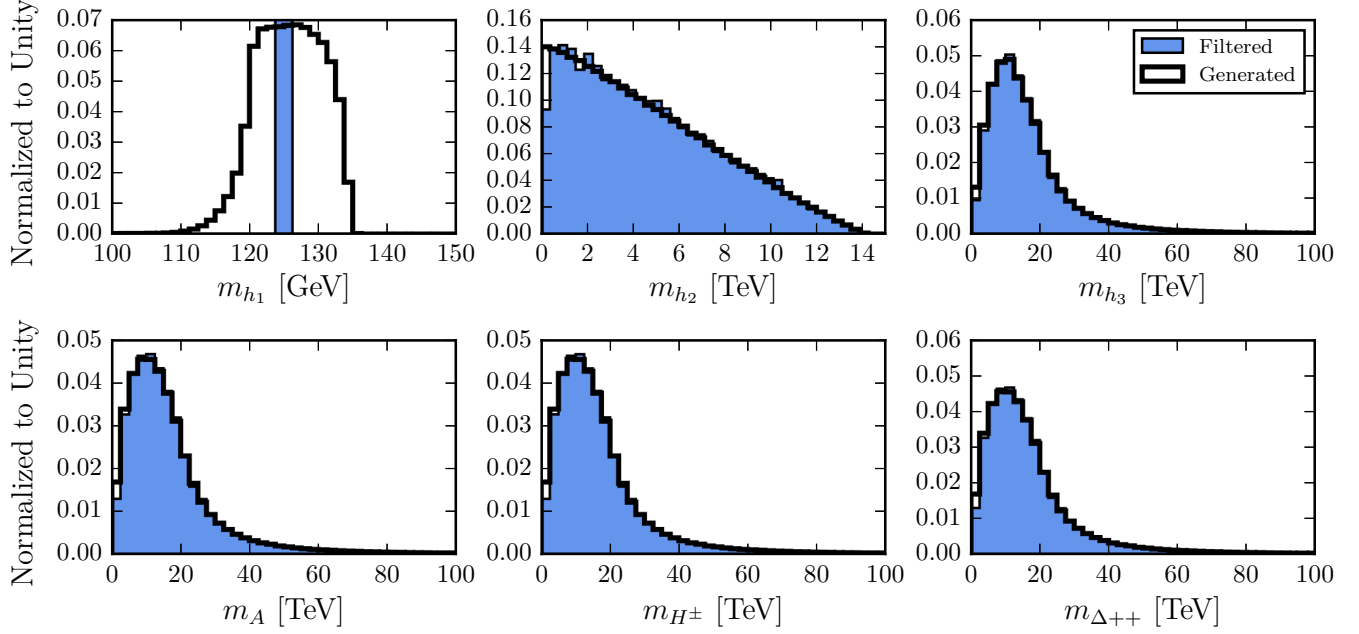


FIG. 1. Distribution of the physical masses in the general scan. Parameters are varied as in Table II.

TABLE I. Characterization of the three benchmark under study, giving the composition of h_2 .

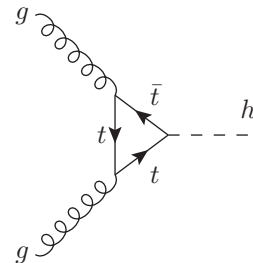
Benchmark	Composition of h_2	$ O_\chi^{21} $	$ O_\chi^{22} $	$ O_\chi^{23} $
B1	mostly triplet	1.0×10^{-5}	1.5×10^{-3}	1.0
B2	mostly singlet	1.0	9.7×10^{-3}	8.7×10^{-4}
B3	mixed	8.9×10^{-1}	9.8×10^{-4}	4.6×10^{-1}

TABLE II. Scanned range for the independent parameters and their values for the different benchmarks.

Parameter	Scanned Range	B1	B2	B3	Units
v_σ	[0, 5000]	1500	3300	2500	GeV
v_ϕ	[245, 247]	246	246	246	GeV
v_Δ	[0, 0.35]	0.2	0.2	0.3	GeV
λ_1	[0.127, 0.15]	0.13	0.13	0.13	-
λ_2	[-4, 4]	0.1	0.1	0.1	-
λ_3	[-4, 4]	0.1	0.1	0.1	-
λ_4	[-4, 4]	0.1	0.1	0.1	-
λ_5	[-4, 4]	1.0	0.5	0.8	-
β_1	[0, 4]	0.3	0.02	0.008	-
β_2	[-0.05, 0.05]	0.02	0.005	0	-
β_3	[-4, 4]	0.1	0.5	0.6	-
κ	[0, 1]	0.001	0.0015	0.0004	-

TABLE III. Physical masses in GeV for the different benchmarks.

Parameter	B1	B2	B3
m_{h_1}	125	125	125
m_{h_2}	476	660	316
m_{h_3}	1162	865	318
m_A	476	865	317
m_{H^\pm}	460	861	298
$m_{\Delta^{++}}$	443	857	277



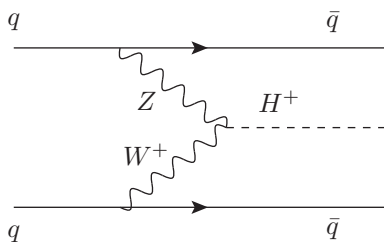
This process dominates SM-like Higgs production not only because the htt coupling is large, but also because the parton distribution functions indicate that it is easier to find a gluon inside the proton than a heavy quark or an electroweak gauge boson.

Nevertheless, this mechanism is not efficient for a not-mainly-doublet Higgs boson (which is the case for h_2 and A in our model benchmarks), because that Higgs couples to quarks very weakly. In the model studied here, the ratio of production cross-sections in the gluon-gluon fusion mode for h_1 and h_2 is,

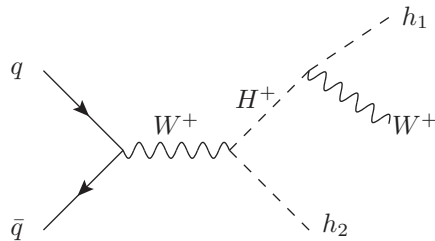
$$\frac{\sigma(ggF, h_2)}{\sigma(ggF, h_1, m_{h_1} = m_{h_2})} = \left(\frac{O_\chi^{22}}{O_\chi^{12}} \right)^2 \approx (O_\chi^{22})^2. \quad (12)$$

The last approximation is valid because we have h_1 mainly doublet (SM-like). The production cross-section at $\sqrt{s} = 14$ TeV for h_2 reaches 5.7×10^{-6} pb in B1, 5.7×10^{-5} pb in B2 and 3.9×10^{-6} pb in B3. For A production, the above ratio is proportional to $(O_\phi^{32})^2$ and we get similar numbers. The cross-section at $\sqrt{s} = 14$ TeV reaches 6.8×10^{-6} pb in B1, 4.0×10^{-7} pb in B2 and is somewhat higher in B3, reaching 2.5×10^{-5} pb. So we conclude that the above ratio is around 10^{-4} at most. This is why, if the model is correct, we may have not seen h_2 (nor A) at the LHC via ggF , as is not a dominant production mode since h_2 does not behave like a SM-like Higgs.

Other production mechanisms that can be relevant at the LHC are electroweak modes, for example vector boson fusion (VBF), but they also produce small cross-sections for our given benchmarks. When considering the sum over all VBF processes like the diagram below, the highest cross-section at $\sqrt{s} = 14$ TeV we get is 2.5×10^{-5} pb for the charged Higgs production,



in B3. Production processes via quark anti-quark annihilation can also be relevant. In the case of h_2 production, the highest contribution comes from the diagram



for B1 and B3. The cross-section at $\sqrt{s} = 14$ TeV for B1 is 4.5×10^{-4} pb. Production of A at $\sqrt{s} = 14$ TeV dominates in B1 when in the above diagram we replace h_2 with A , W^+ with a Z , h_1 also with a Z and H^+ with h_2 , leading to the AZZ final state. This gives a cross-section of 3.7×10^{-4} pb. It can go higher in B3 in the AJJ final state, with a cross-section reaching 2.3×10^{-3} pb. Charged Higgs production at $\sqrt{s} = 14$ TeV can reach 4.3×10^{-3} pb in B3 in the $H^+W^-W^-$ final state (replacing W^+ and h_1 with W^- , H^+ with Δ^{--} and h_2 with H^+ in the above diagram).

The highest cross-section found in our model benchmarks for each characteristic production mechanism at the LHC is summarized in Table IV for comparison.

TABLE IV. Highest LHC production cross-section (in units of pb) found in our benchmarks for h_2 , A and H^\pm at $\sqrt{s} = 14$ TeV via the three characteristic production mechanisms: ggF , VBF and $q\bar{q}$ annihilation.

σ	h_2	A	H^\pm
ggF	5.7×10^{-5} (B2)	2.5×10^{-5} (B3)	—
VBF	4.4×10^{-6} (B3)	2.2×10^{-5} (B1)	2.5×10^{-5} (B3)
$q\bar{q}$	4.5×10^{-4} (B1)	2.3×10^{-3} (B3)	4.3×10^{-3} (B3)

To finish, not even the HL-LHC [30] will help, because it is expected to have a factor of 10 increase in luminosity, and it will not compensate the smallness of the production cross-section.

In summary, it seems hadron colliders are not well equipped to produce the new states h_2 , A and H^\pm . Production for h_2 and A via ggF at the LHC is not efficient since these Higgs bosons are not-mainly doublet. Productions for h_2 , A and H^\pm via VBF can be only as large as $\sim 10^{-5}$ pb for our benchmarks. Electroweak production via quark anti-quark annihilation can be as high as $\sim 10^{-3}$ pb. Given that our benchmarks are not likely to be observed at the LHC (a dedicated analysis is needed to confirm this), the large hadronic background at the LHC and the advantage of a cleaner collider environment at lepton colliders, we focus on the production for these states at future electron-positron colliders.

V. PRODUCTION AT e^+e^- COLLIDERS

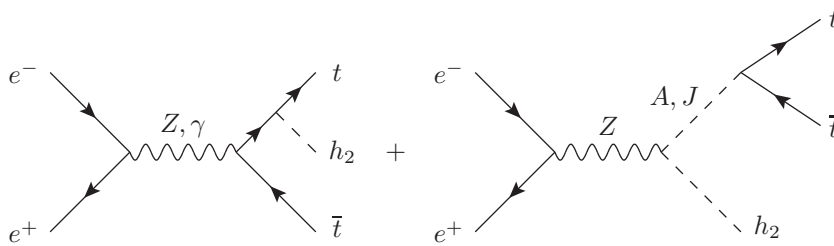
In order to assess the discovery potential of the model, we implement it in FEYNRULES [28] so we can extract relevant parameters and Feynman rules. We then interface the output to the MADGRAPH5 [29] event generator in order to compute production cross-sections, as we did in the previous section.

The FCC-ee machine is a hypothetical circular e^+e^- collider at CERN with a high luminosity but low energy, designed to study with precision the Higgs boson [31]. We consider its highest projected energy 350 GeV with a luminosity of 2.6 ab^{-1} , which was calculated by taking the 0.13 ab^{-1} quoted in [31] and assuming 4 interaction points and 5 years of running of the experiment.

The canonical program for the ILC [32] includes three CM energies given by 250 GeV, 500 GeV, and 1000 GeV, with integrated luminosities 250 fb^{-1} , 500 fb^{-1} and 1000 fb^{-1} , respectively. CLIC [33] has three operating CM energies: $\sqrt{s} = 350 \text{ GeV}$, 1.4 TeV and 3 TeV, with estimated luminosities 500 fb^{-1} , 1.5 ab^{-1} and 2 ab^{-1} , respectively. Based on this, we compute e^+e^- production cross-sections for h_2 , A and H^+ for our three benchmarks at different CM energies.

A. h_2 Production

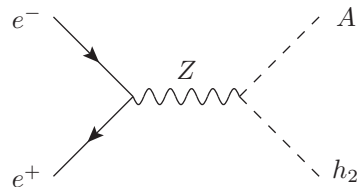
Table V shows h_2 production cross-sections at e^+e^- colliders, prospected luminosities and CM energies for the FCC-ee, ILC and CLIC colliders. The cross-sections are calculated by summing all $e^+e^- \rightarrow h_2XY$ 3-body production modes, plus the 2-body production modes



plus a similar graph with h_2 emitted from the anti-quark and another graph with the A boson being replaced by a Z boson. This production process is enhanced when the A scalar boson is on-shell, $e^+e^- \rightarrow h_2A \rightarrow h_2t\bar{t}$, corroborated by the fact that $B(A \rightarrow t\bar{t}) = 0.5$ is large for B1, as shown in Table IX.

In the central frame of Fig. 2 we see B2. In this case, production cross-sections are systematically smaller be-

$e^+e^- \rightarrow h_2X$, where X is a particle that does not decay. The production cross-sections shown in Table V are dominated by the 2-body production process (or mode) $e^+e^- \rightarrow h_2A$ and by 3-body production processes as follows. In B1 the process $e^+e^- \rightarrow h_2t\bar{t}$ is the most important one. In B2 the dominating process is $e^+e^- \rightarrow h_2Ah_1$. In B3 the process $e^+e^- \rightarrow h_2Zh_1$ is the dominant one. All of them are enhanced when a second heavy particle is also on-shell. We show in Fig. 2 the main h_2 production modes for all 3 benchmarks. In B1 (left frame) this particle is potentially observed at CLIC only when the A scalar is also on-shell. Thus, the main 2-body production mode is the so-called associated production,



defined when h_2 is produced together with an A . The coupling ZAh_2 is given in Appendix B. Since A is mainly triplet, O_φ^{33} is of order 1. In addition, in B1 h_2 is mainly triplet, thus O_χ^{23} is also of order 1. Therefore, the whole coupling ZAh_2 is not suppressed with respect to the gauge coupling g .

The most important 3-body production modes in B1 are also displayed in the left frame of Fig. 2. The main production process is $h_2t\bar{t}$ when A is on-shell. Diagrammatically it looks like,

cause in this benchmark h_2 is mainly singlet and couplings to gauge bosons are smaller. Also the main production modes are different. The process $e^+e^- \rightarrow h_2t\bar{t}$ is no longer efficient, with a cross-section of the order of 10^{-8} pb and outside of the plot. The reason is that the coupling Zh_2A is small when h_2 is mainly singlet. The main production mode for B2 is $e^+e^- \rightarrow h_2Ah_1$, with Feynman diagrams for the sub-processes given by,

TABLE V. Production cross-section (in units of ab) for h_2 at an e^+e^- collider for projected energies in the 3 benchmarks. Estimated luminosities are also given in units of ab^{-1} .

\sqrt{s} [TeV]	\mathcal{L}_{FCCee}	\mathcal{L}_{ILC}	\mathcal{L}_{CLIC}	B1: σ	B2: σ	B3: σ
0.250	-	0.25	-	0	0	0
0.350	2.6	-	0.5	0	0	1.7×10^{-5}
0.500	-	0.5	-	3.1×10^{-6}	0	2.5×10^{-2}
1.0	-	1	-	1.4×10^3	0.9	3.7×10^3
1.4	-	-	1.5	1.1×10^4	3.6	4.1×10^3
3	-	-	2	6.1×10^3	3.5×10^{-2}	2.0×10^3

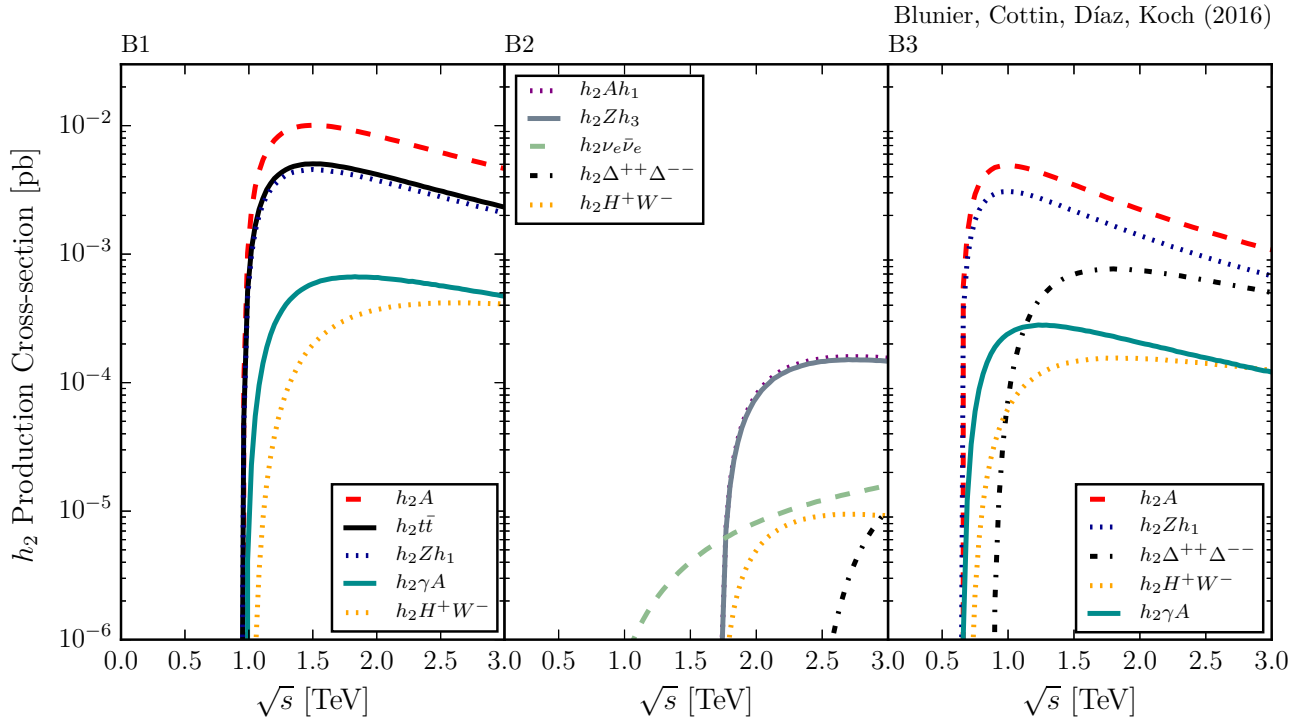
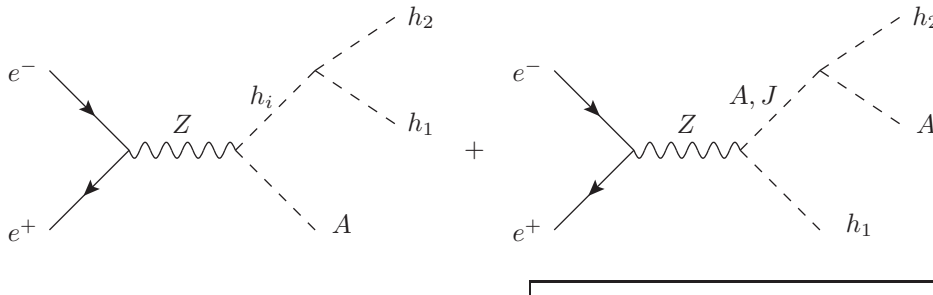


FIG. 2. Production modes for h_2 at an e^+e^- collider in the 3 benchmarks. The legend shows the final state after the e^+e^- collision.

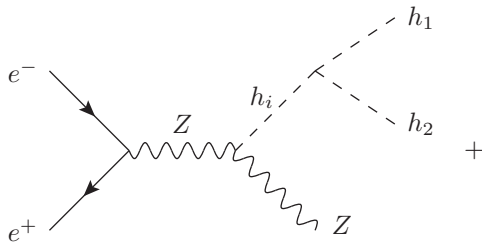


plus Feynman diagrams where in the last sub-process we replace (A, J) by Z and/or interchange h_1 with h_2 . This mode is enhanced when h_3 is on-shell, since in B2 h_3 is

mainly triplet and the coupling ZAh_3 is large resulting in $e^+e^- \rightarrow h_3A \rightarrow h_2h_1A$.

B3 is an intermediate situation. Even in this case, h_2

production cross-sections are potentially observable when A is also on-shell. The production cross-section $e^+e^- \rightarrow$

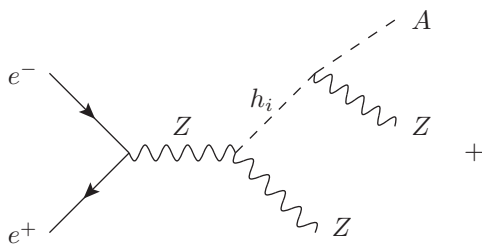


where $i = 1, 2, 3$, and missing are a graph with the CP -odd scalar replaced by a Z and one formed with a ZZh_1h_2 quartic coupling. This production mode is enhanced when the A boson is on-shell, $e^+e^- \rightarrow h_2A \rightarrow h_2h_1Z$, with a branching fraction $B(A \rightarrow h_1Z) = 0.9$ as shown in Table IX.

Fig. 3 shows a scan for the production mode $e^+e^- \rightarrow h_2t\bar{t}$ (left frame) and $e^+e^- \rightarrow h_2h_1A$ (right frame), two of the important 3-body h_2 production modes. In the case of $e^+e^- \rightarrow h_2t\bar{t}$, the production cross-section reaches up to 0.01 pb. The largest cross-sections are seen when h_2 is mainly triplet (black triangular points), with a typical value between 0.001 and 0.01 pb. B1 is shown as a black solid curve. The value of the cross-section drops when h_2 is mainly singlet (orange star points), with values typically smaller than 10^{-4} pb. This is because a singlet does not couple to the Z gauge boson. The chosen B2 lies within the cloud of points. The case where h_2 is mixed is much more rare and no point has been generated in this scenario due to its fine-tuned character.

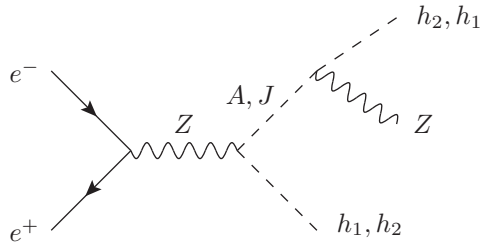
The case of $e^+e^- \rightarrow h_2Ah_1$ is shown in the right frame of Fig. 3. This is the main process in B2, where h_2 is mainly singlet (orange star points). In this case, cross-sections can reach up to 10^{-3} pb, but can also be as low as 10^{-14} pb, depending on whether h_3 is on-shell or not. In the case where h_2 is mainly triplet (black triangular points) the cross-section is more restricted. It can vary between 10^{-3} and 10^{-8} pb and B1 is a very typical case. Cross-sections are larger when an intermediate heavy scalar is also on-shell.

Notice that the popular modes for the production of



It is enhanced when h_2 is on-shell, with a branching frac-

h_2A is smaller than in B1, but still large. The main 3-body production mode in this case is $e^+e^- \rightarrow h_2Zh_1$, with sub-processes given by,

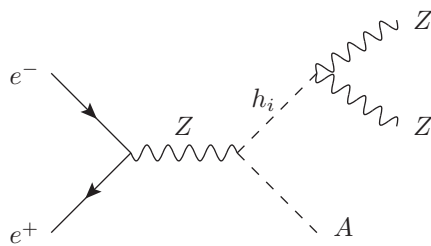


a SM-like Higgs boson in a e^+e^- collider, known collectively as vector boson fusion, $e^+e^- \rightarrow h_2e^+e^-$ (fusion of two Z bosons) or $e^+e^- \rightarrow h_2\nu_e\bar{\nu}_e$ (fusion of two W bosons) do not work in our case because the h_2 couplings to vector bosons are suppressed by the triplet vev v_Δ . In addition, most of the charged leptons go through the beam pipe, thus $\sigma(e^+e^- \rightarrow h_2e^+e^-)$ is further penalized when a cut on the charged lepton pseudo-rapidity is imposed. We use MADGRAPH5 default cuts, which impose that the absolute value of the charged lepton pseudo-rapidity is smaller than 2.5.

B. A Production

Table VI shows A production at e^+e^- colliders, prospected luminosities and CM energies for the FCC-ee, ILC and CLIC colliders. The cross-sections are calculated in the same manner explained before. In B1 and B2 the dominating process is $e^+e^- \rightarrow AZZ$, and in B3 the dominating process is $e^+e^- \rightarrow AJJ$, and all of them are enhanced when a second heavy particle is also on-shell.

Fig. 4 shows the production cross-sections for an A boson. In B1 (left frame) A is potentially observable at CLIC when produced in association with an h_2 . In this case the mode $e^+e^- \rightarrow Ah_1$ is suppressed because O_φ^{32} and O_χ^{13} are both small (see Feynman rule in Appendix B), thus the coupling h_1AZ itself is suppressed with respect to g . Three body production modes are also in Fig. 4. The dominant 3-body production mode in B1 is $e^+e^- \rightarrow AZZ$, represented by the Feynman diagrams,



tion $B(h_2 \rightarrow ZZ) = 0.6$, as indicated in Table VIII. As

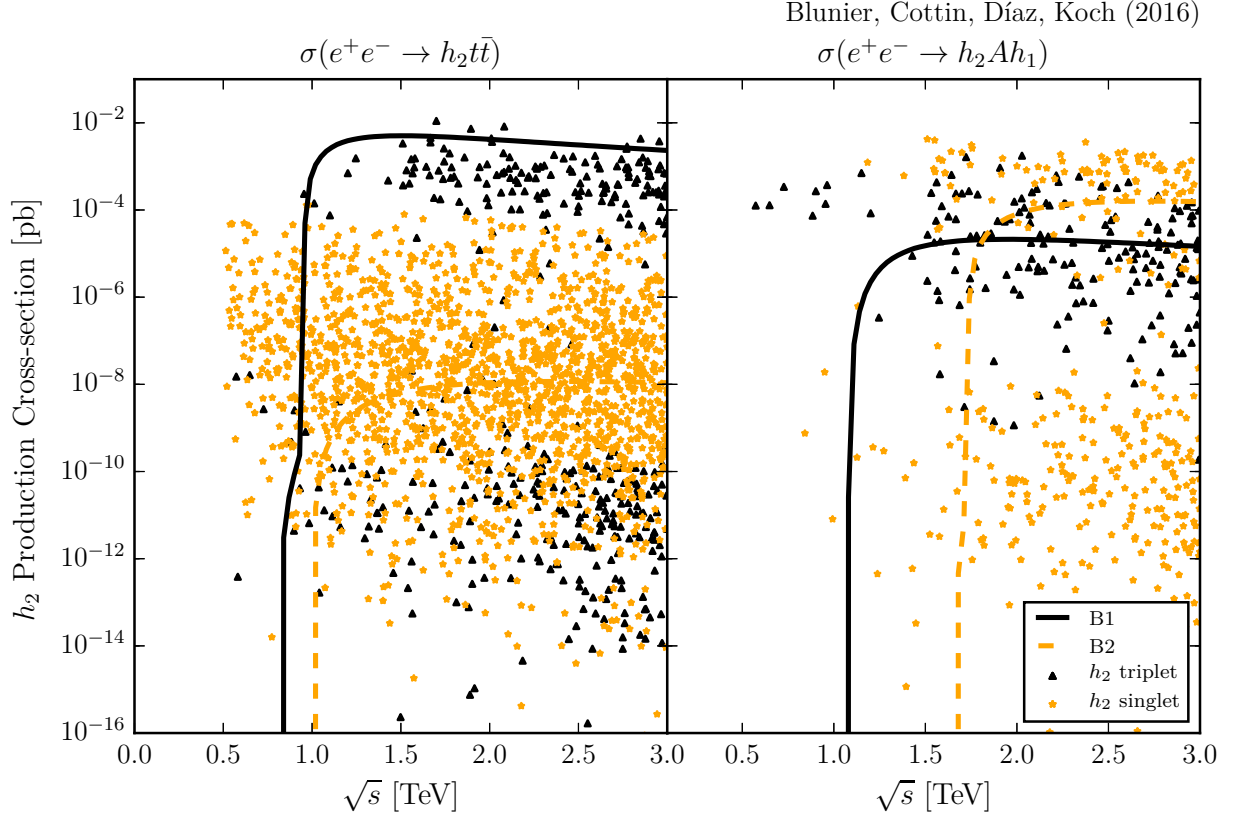


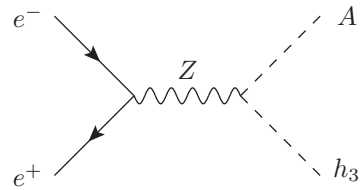
FIG. 3. Production modes $e^+e^- \rightarrow h_2 t \bar{t}$ and $e^+e^- \rightarrow h_2 h_1 A$.

TABLE VI. Production cross-section (in units of ab) for A at an e^+e^- collider for projected energies in the 3 benchmarks. Estimated luminosities are also given in units of ab^{-1} .

\sqrt{s} [TeV]	\mathcal{L}_{FCCee}	\mathcal{L}_{ILC}	\mathcal{L}_{CLIC}	B1: σ	B2: σ	B3: σ
0.250	-	0.25	-	0	0	0
0.350	2.6	-	0.5	0	0	1.4×10^{-10}
0.500	-	0.5	-	1.5×10^{-12}	0	1.5×10^{-2}
1.0	-	1	-	1.4×10^3	2.2×10^{-5}	2.5×10^4
1.4	-	-	1.5	1.1×10^4	3.5×10^{-3}	2.1×10^4
3	-	-	2	6.2×10^3	3.6×10^3	7.5×10^3

explained later in the decay Section, the coupling $h_2 ZZ$ is large if h_2 is mainly triplet (B1).

In B2 the CP -even Higgs boson created in association with A is no longer h_2 but h_3 . If h_2 is mainly singlet, h_3 is mainly triplet, and the coupling ZAh_3 is not suppressed. This is confirmed in the central frame of Fig. 4 where we have B2. The most important 2-body production mode is precisely $e^+e^- \rightarrow Ah_3$, represented by the Feynman diagram



Also in the central frame of Fig. 4 we see the main 3-body A production modes. The most important one is again $e^+e^- \rightarrow AZZ$, and it is enhanced when h_3 is on-shell.

B3 is an intermediate case, and we can see in the right

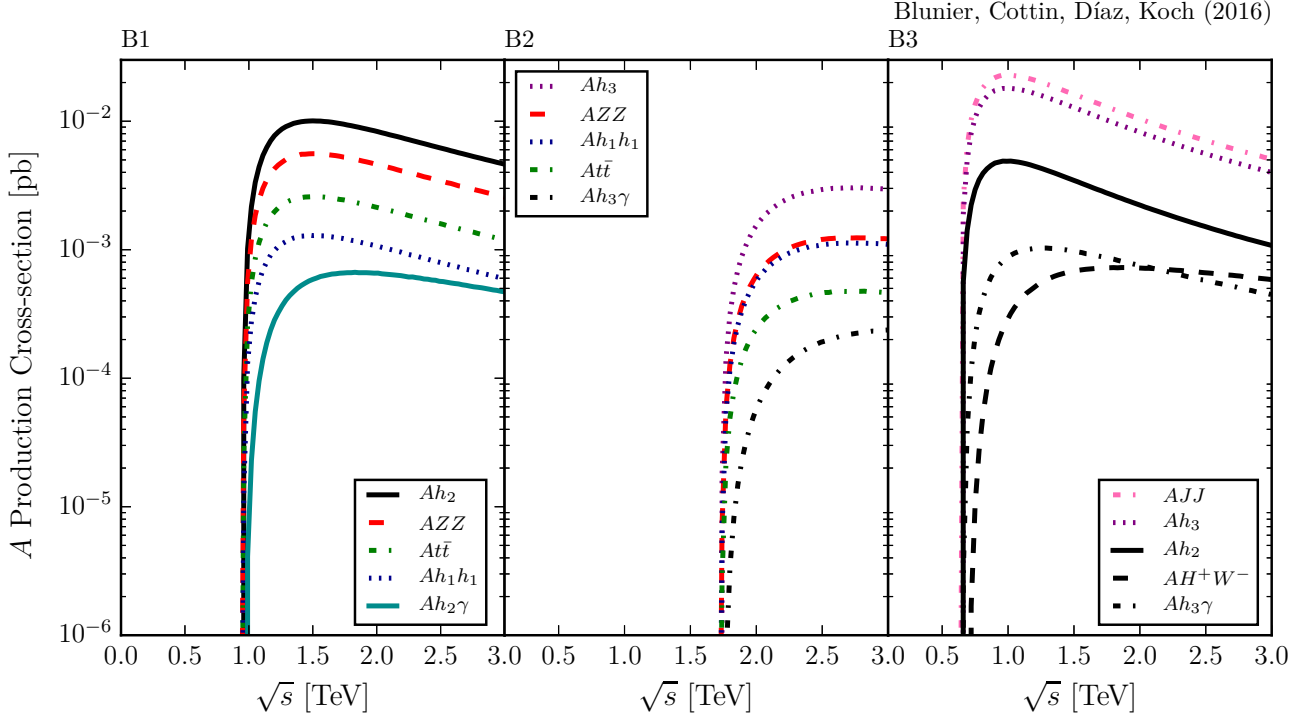
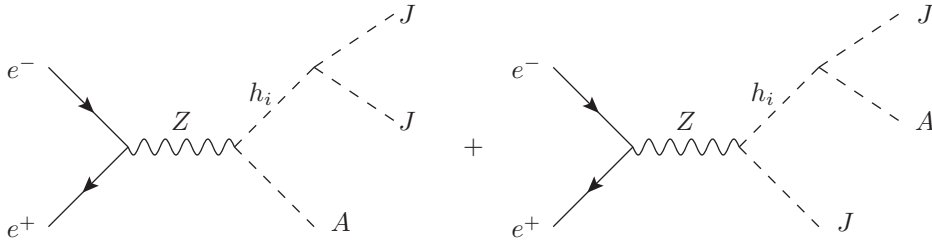


FIG. 4. Production modes for A at an e^+e^- collider in all 3 benchmarks. The legend shows the final state after the e^+e^- collision.

frame of Fig. 4 that the two 2-body production modes $e^+e^- \rightarrow Ah_2$ and $e^+e^- \rightarrow Ah_3$ are important since both

h_2 and h_3 have a large triplet component. Among the 3-body production modes, the largest one is $e^+e^- \rightarrow AJJ$,



and it is enhanced when h_2 and h_3 are on-shell.

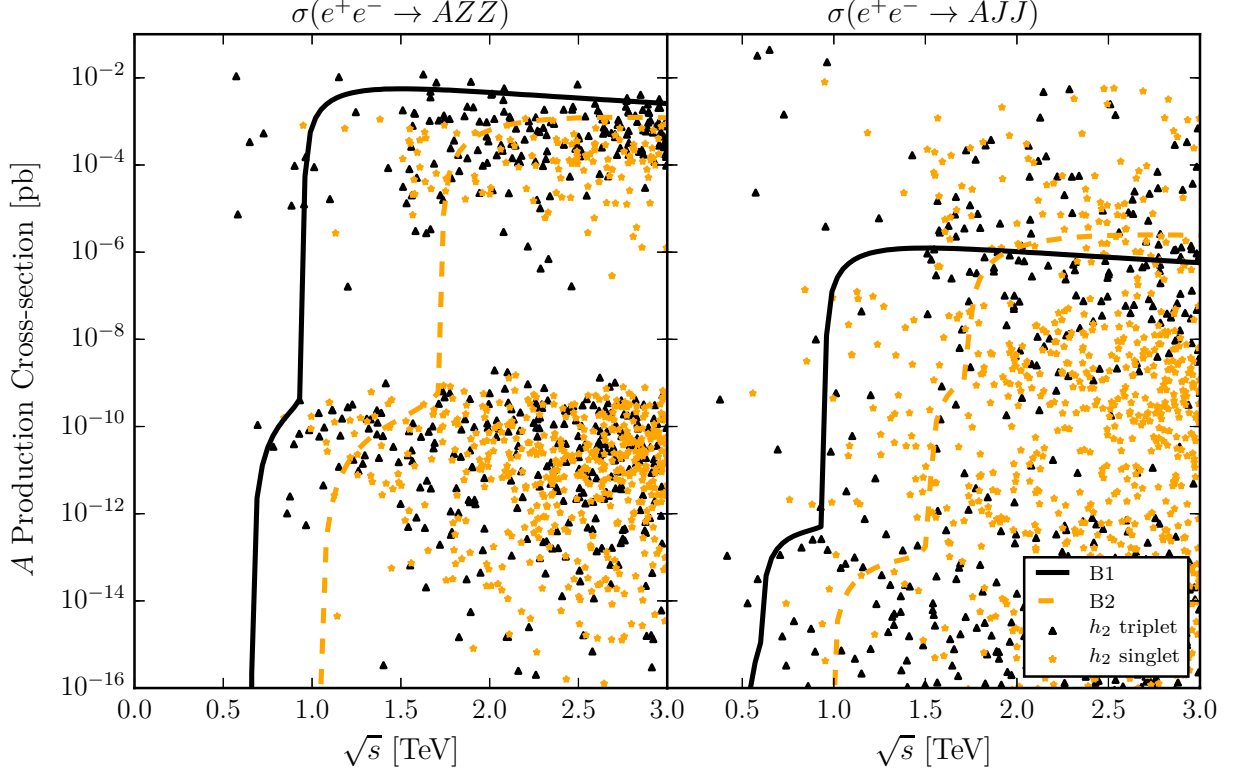
Fig. 5 shows scans for the process $e^+e^- \rightarrow AZZ$ (left frame), important for B1 and B2, and the process $e^+e^- \rightarrow AJJ$ (right frame), important in B3. In the first case, the production cross-section is increased when h_2 is also on-shell, as explained before. The cross-section is not larger than 0.01 pb, and B1 is not far below from that value. In the last process a triple scalar coupling is important, and the exact values of the parameters in the potential are crucial. In this case, B3 is characterized by a large value of β_3 which increases the coupling h_3JJ . As before, in Fig. 5 we include the curves corresponding to each benchmark to facilitate comparisons.

C. H^+ Production

Table VII shows H^+ production cross-sections at e^+e^- colliders, prospected luminosities and CM energies for the FCC-ee, ILC and CLIC colliders. Besides the 2-body production cross-section for $e^+e^- \rightarrow H^+H^-$, in B1 and B2 the 3-body process $e^+e^- \rightarrow H^+h_1W^-$ dominates. In B3 the process $e^+e^- \rightarrow H^+W^+\Delta^{--}$ dominates. The last case presents a high interest, as the doubly charged Higgs boson gives us an independent window to study neutrinos.

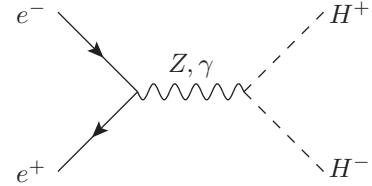
Fig. 6 shows the 2-body and 3-body production of an H^+ boson. The charged Higgs boson is potentially ob-

Blunier, Cottin, Díaz, Koch (2016)

FIG. 5. Production modes $e^+e^- \rightarrow AZZ$ and $e^+e^- \rightarrow AJJ$.TABLE VII. Production cross-section (in units of ab) for H^+ at an e^+e^- collider for projected energies in the 3 benchmarks. Estimated luminosities are also given in units of ab^{-1} .

\sqrt{s} [TeV]	\mathcal{L}_{FCCee}	\mathcal{L}_{ILC}	\mathcal{L}_{CLIC}	B1: σ	B2: σ	B3: σ
0.250	-	0.25	-	0	0	0
0.350	2.6	-	0.5	0	0	5.8×10^{-3}
0.500	-	0.5	-	1.9×10^{-4}	0	0.5
1.0	-	1	-	1.6×10^3	4.1×10^{-3}	1.7×10^4
1.4	-	-	1.5	7.0×10^3	3.5×10^{-2}	1.5×10^4
3	-	-	2	5.0×10^3	2.4×10^3	6.6×10^3

servable at CLIC when produced in association with another H^- , represented by the graph,



The couplings $H^+H^-\gamma$ and H^+H^-Z are both of the order of electroweak couplings, as can be seen in Appendix B. Among the 3-body modes, in B1 and B2 the main production mode is $e^+e^- \rightarrow H^+h_1W^-$, represented by the sub-processes,

Blunier, Cottin, Díaz, Koch (2016)

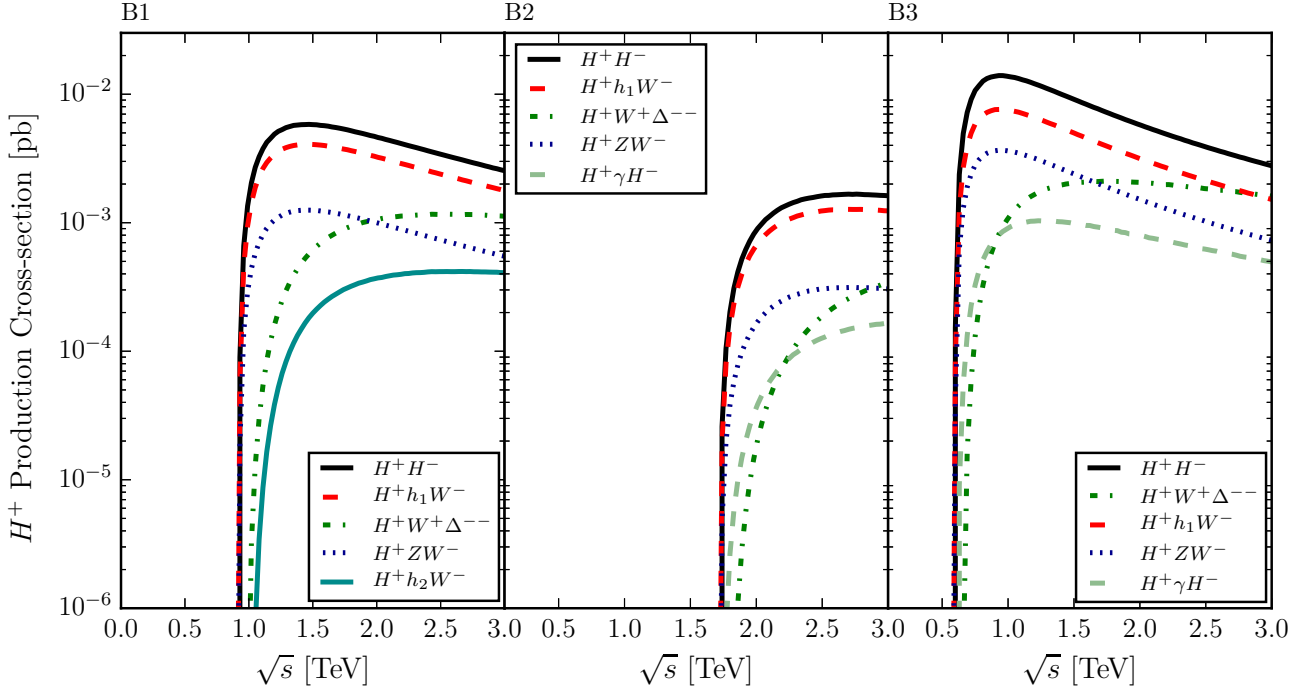
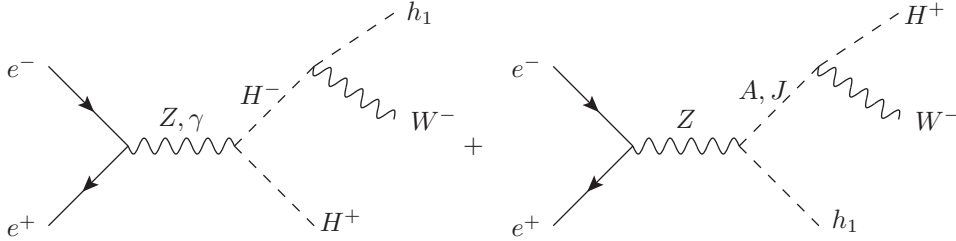


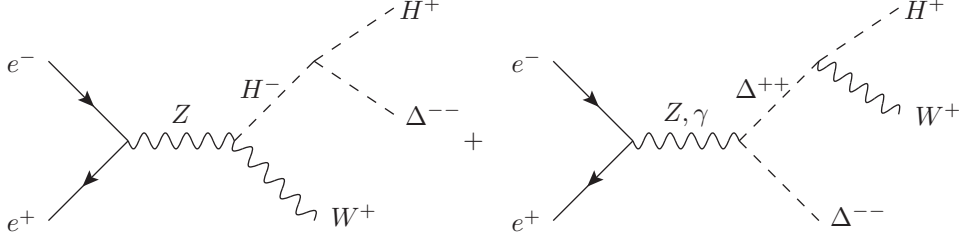
FIG. 6. Production modes for H^+ at an e^+e^- collider in all 3 benchmarks. The legend shows the final state after the e^+e^- collision.



plus a graph where the intermediate charged Higgs is replaced by a W and removing the intermediate photon, graphs where the external charged Higgs and the W are interchanged (also removing the photon), a graph where (A, J) is replaced by a Z , graphs that involve quartic couplings, and a graph with a neutrino in the t -channel. This mode is dominated by the graph where the charged

Higgs is on-shell. Note that the coupling ZH^+W^- is suppressed by the triplet vev. This mode is enhanced when H^- is also on-shell, corroborated by the fact that $B(H^- \rightarrow h_1W^-) = 0.8$ in B2.

Similarly, in Fig. 6 we see that the mode $e^+e^- \rightarrow H^+W^+\Delta^{--}$ dominates in B3. It is represented by,



plus a graph where the external particles H^+ and Δ^{--} are interchanged and at the same time the intermediate Δ^{++} is replaced by H^- , plus two graphs where the H^- is replaced by a W^- with Z exchanged for a photon, and two graphs with quartic couplings. As it was mentioned before, the production of a Δ^{++} is important because it could lead to the observation of its decay into two charged leptons, which could probe the mechanism for neutrino masses.

Fig. 7 shows a general scan for the 3-body production modes $e^+e^- \rightarrow H^+h_1W^-$ (left frame) and $e^+e^- \rightarrow H^+W^+\Delta^{--}$ (right frame). For the case $e^+e^- \rightarrow H^+h_1W^-$, the majority of the scenarios give a cross-section between 10^{-2} and 10^{-4} pb, as long as a second heavy particle is also on-shell. In the case of $e^+e^- \rightarrow H^+W^+\Delta^{--}$, the cross-section is of the same order between 10^{-3} and 10^{-5} pb, also independent of the composition of h_2 . If neutrinos acquire their mass via a coupling to the triplet, the mechanism can be probed through the production of a double charged Higgs boson.

VI. DECAY BRANCHING FRACTIONS

In this Section, we study the decay modes of the SM-like Higgs boson h_1 , the next-to heaviest Higgs h_2 , the CP -odd Higgs A , and the charged Higgs H^\pm . For the computation of branching fractions, we consider $B = \Gamma(H \rightarrow (XX)_i) / \sum_i \Gamma(H \rightarrow (XX)_i)$, with $H = h_1, h_2, A, H^\pm$. For the CP -even Higgses we have $XX = \tau\bar{\tau}, b\bar{b}, WW, ZZ, \gamma\gamma, Z\gamma, gg, JJ, JZ$ for h_1 and we include $t\bar{t}$ and h_1h_1 to the previous list for h_2 . For A we consider $XX = \tau\bar{\tau}, b\bar{b}, t\bar{t}, h_iZ, h_iJ, \gamma\gamma, Z\gamma, gg$, with $i = 1, 2$. For H^\pm , we have $XX = t\bar{b}, h_iW^\pm, JW^\pm, ZW^\pm$, with $i = 1, 2$.

We define

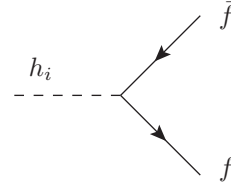
$$\lambda(a, b, c) = a^2 + b^2 + c^2 - 2ab - 2ac - 2bc. \quad (13)$$

In the special case $b = c$, it is reduced to the function β ,

$$\beta(b/a) = \frac{1}{a} \lambda^{1/2}(a, b, b) = \sqrt{1 - 4\frac{b}{a}}. \quad (14)$$

A. h_1 and h_2 Decays

We first mention the decay modes to fermions for h_i ($i = 1, 2$), which include $h_i \rightarrow b\bar{b}$ and $h_i \rightarrow \tau\bar{\tau}$. The decay $h_2 \rightarrow t\bar{t}$ is considered for h_2 , but not for h_1 . The corresponding Feynman diagram is



with Feynman rule given in Appendix B.

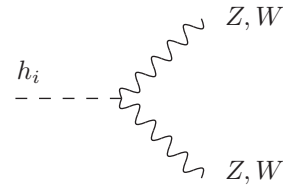
The decay widths are given by

$$\Gamma(h_i \rightarrow f\bar{f}) = \frac{N_c m_{h_i}}{8\pi} \beta^3(m_f^2/m_{h_i}^2) |\lambda_{h_i f f}|^2, \quad (15)$$

where the number of colors is $N_c = 3$ for quarks and $N_c = 1$ for leptons. We define the coupling $\lambda_{h_i f f} = O_\chi^2 h_f / \sqrt{2}$, where h_f corresponds to the respective Yukawa coupling in the convention $m_f = h_f v_\phi / \sqrt{2}$.

Since h_1 is always mainly doublet and h_2 is not, decay rates of h_1 to fermions are consistently larger than decay rates of h_2 to fermions. Similarly, since the h_2 component to doublet is larger in B2 compared to B1 and B3, the corresponding decay rate is larger too.

Also important are the vector boson decays $h_i \rightarrow W^+W^-$, $h_i \rightarrow ZZ$, with Feynman diagram,



The decay rate where both gauge bosons are on-shell is

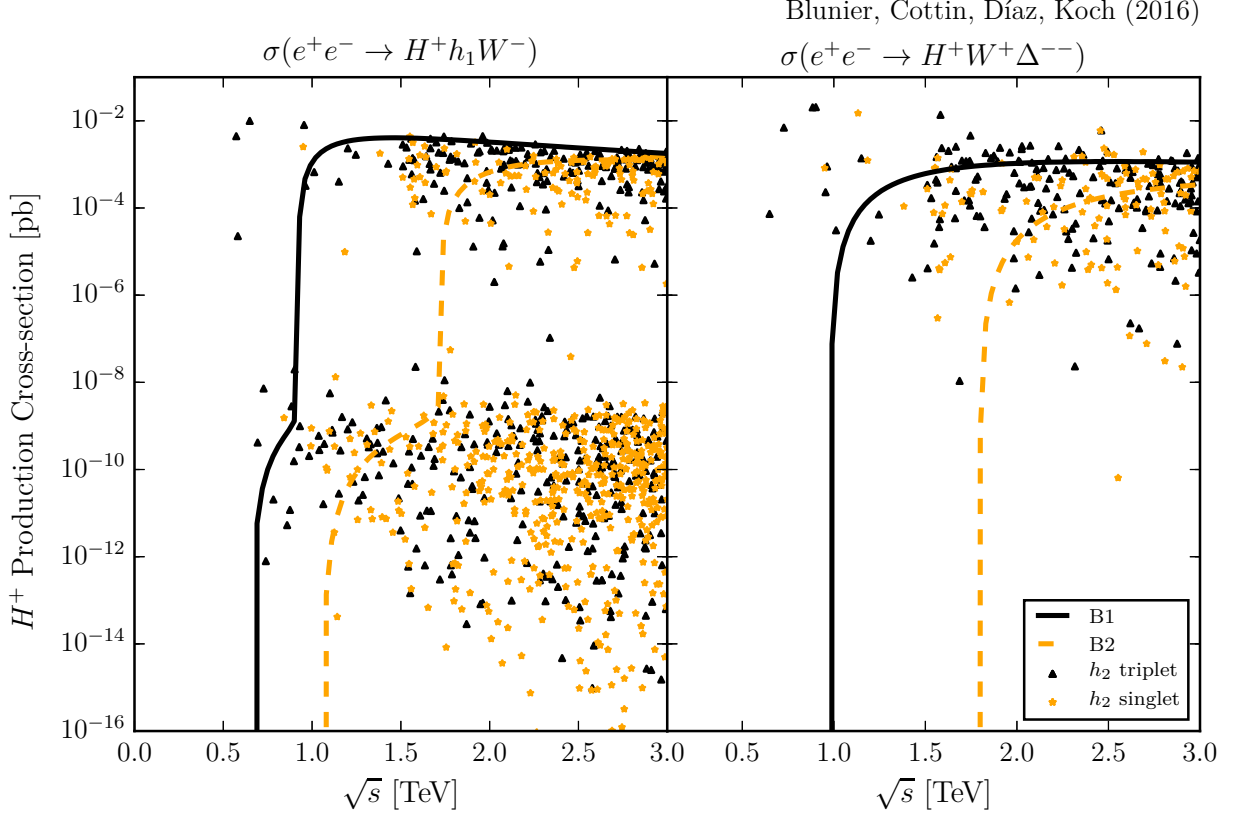


FIG. 7. Production modes $e^+e^- \rightarrow H^+h_1W^-$ and $e^+e^- \rightarrow H^+W^+\Delta^{--}$.

$$\Gamma(h_i \rightarrow VV) = \frac{m_{h_i}^3 \delta'_V}{128\pi m_V^4} \left[1 - \frac{4m_V^2}{m_{h_i}^2} + \frac{12m_V^4}{m_{h_i}^4} \right] \beta(m_V^2/m_{h_i}^2) |M_{h_i VV}|^2, \quad (16)$$

with $V = Z, W$, $\delta'_W = 2$ and $\delta'_Z = 1$. The decay rate where one vector boson is off-shell is

$$\Gamma(h_i \rightarrow VV^*) = \frac{3g_V^2 m_{h_i} \delta_V}{512\pi^3 m_V^2} F(m_V/m_{h_i}) |M_{h_i VV}|^2, \quad (17)$$

with $g_W = g$, $g_Z = g/c_W$, $\delta_W = 1$, and $\delta_Z = \frac{7}{12} - \frac{10}{9}s_W^2 + \frac{40}{27}s_W^4$, where s_W and c_W are the sine and cosine of the Weinberg angle. The F function is defined in [34]. The relevant couplings (with units of mass) can be read from Appendix B, from where we define

$$M_{h_i WW} = \frac{1}{2}g^2(O_\chi^{i2}v_\phi + 2O_\chi^{i3}v_\Delta), \quad (18)$$

$$M_{h_i ZZ} = \frac{1}{2}(g^2 + g'^2)(O_\chi^{i2}v_\phi + 4O_\chi^{i3}v_\Delta), \quad (19)$$

and use them in eq. (16) and eq. (17). In the case of h_2 , since the penalization due to vev is already large ($v_\Delta/v_\phi \sim 10^{-3}$ for our benchmarks), the h_2 component to doublet becomes important. Thus, the couplings $h_2 VV$ are larger for B2, and in turn the decay rate (and branching fractions).

The decay to $\gamma\gamma$ is given by [18, 35],

$$\begin{aligned} \Gamma(h_i \rightarrow \gamma\gamma) &= \frac{\alpha^2 g^2}{1024\pi^3} \frac{m_{h_i}^3}{m_W^2} \left| F_0(\tau_{H^+}^i) \frac{m_W}{m_{H^+}^2} M_{h_i H^+ H^-} \right. \\ &\quad + 4F_0(\tau_\Delta^i) \frac{m_W}{m_{\Delta^{++}}^2} M_{h_i \Delta^{++} \Delta^{--}} \\ &\quad + F_1(\tau_W^i) \frac{1}{m_W} M_{h_i WW} \\ &\quad \left. + \frac{4\sqrt{2}}{3h_t} F_{1/2}(\tau_t^i) \lambda_{h_i tt} \right|^2, \quad (20) \end{aligned}$$

where the couplings $M_{h_i H^+ H^-}$ (in our convention $H^+ \equiv h_2^+$), $M_{h_i \Delta^{++} \Delta^{--}}$, and $M_{h_i WW}$ are defined in Appendix B and in eq. (18). In eq. (20) we have defined $\tau_a^i = 4m_a^2/m_{h_i}^2$ where $a = H^+, \Delta, W$. The F_0, F_1 and $F_{1/2}$ functions are defined in [34].

The decay to $Z\gamma$ is given by [18, 35]

$$\Gamma(h_i \rightarrow Z\gamma) = \frac{\alpha g^2}{2048\pi^4 m_W^4} |A|^2 m_{h_i}^3 \left(1 - \frac{m_Z^2}{m_{h_i}^2}\right)^3, \quad (21)$$

where A is defined as

$$A = A_W + A_t + A_0^{H^+} + 2A_0^{\Delta^{++}}, \quad (22)$$

with

$$\begin{aligned} A_W + A_t &= c_W M_{h_i W W} A_1(\tau_W, \lambda_W) + \frac{g m_W}{c_W} N_c Q_t (1 - 4Q_t s_W^2) \lambda_{h_i t t} A_{1/2}(\tau_t, \lambda_t) \\ A_0^{H^+} &= \frac{m_W^2}{g s_W m_{H^+}^2} \lambda_{ZH^+ H^-} M_{h_i H^+ H^-} A_0(\tau_{H^+}, \lambda_{H^+}) \\ A_0^{\Delta^{++}} &= \frac{m_W^2}{g s_W m_{\Delta^{++}}^2} \lambda_{Z\Delta^{++}\Delta^{--}} M_{h_i \Delta^{++}\Delta^{--}} A_0(\tau_{\Delta^{++}}, \lambda_{\Delta^{++}}), \end{aligned} \quad (23)$$

where

$$\begin{aligned} \lambda_{ZH^+ H^-} &= -\frac{g}{2c_W} (s_\beta^2 - 2s_W^2), \\ \lambda_{Z\Delta^{++}\Delta^{--}} &= -\frac{g}{c_W} (c_W^2 - s_W^2), \end{aligned} \quad (24)$$

as can be seen from Appendix B. The loop functions are,

$$\begin{aligned} A_0(\tau, \lambda) &= I_1(\tau, \lambda), \\ A_1(\tau, \lambda) &= 4(3 - \tan^2 \theta_W) I_2(\tau, \lambda) + [(1 + 2/\tau) \tan^2 \theta_W - (5 + 2/\tau)] I_1(\tau, \lambda), \\ A_{1/2}(\tau, \lambda) &= I_1(\tau, \lambda) - I_2(\tau, \lambda), \end{aligned} \quad (25)$$

with $\tau_b = \frac{4m_b^2}{m_{h_i}^2}$, $\lambda_b = \frac{4m_b^2}{m_Z^2}$, $b = t, W, H^+, \Delta^{++}$, and the parametric integrals I_1, I_2 are specified in [34].

We also consider the 1-loop decay to gg for completeness. It is given by [34]

$$\Gamma(h_i \rightarrow gg) = \frac{\alpha_s^2 g^2 m_{h_i}^3}{128\pi^3 m_W^2} \left| \frac{4\sqrt{2}}{3h_i} F_{1/2}(\tau_t^i) \lambda_{h_i t t} \right|^2 \quad (26)$$

with the $F_{1/2}$ given in Appendix C of [34].

The decay to Majorons $h_i \rightarrow JJ$ and $h_i \rightarrow JZ$ proceeds with a negligible Majoron mass. The decay rates are given by,

$$\Gamma(h_i \rightarrow JZ) = \frac{m_{h_i}^3}{16\pi m_Z^2} |\lambda_{Zh_i J}|^2 \left(1 - \frac{m_Z^2}{m_{h_i}^2} \right)^3 \quad (27)$$

and

$$\Gamma(h_i \rightarrow JJ) = \frac{|M_{h_i JJ}|^2}{32\pi m_{h_i}}, \quad (28)$$

with

$$\lambda_{Zh_i J} = \frac{g}{2c_W} (O_\chi^{i2} O_\varphi^{22} - 2O_\chi^{i3} O_\varphi^{23}). \quad (29)$$

$M_{h_i JJ}$ is defined from the corresponding Feynman rule in Appendix B.

Finally, the decay $h_2 \rightarrow h_1 h_1$ is given by,

$$\Gamma(h_2 \rightarrow h_1 h_1) = \frac{\beta(m_{h_1}^2/m_{h_2}^2)}{32\pi m_{h_2}} |M_{h_2 h_1 h_1}|^2, \quad (30)$$

where $M_{h_2 h_1 h_1}$ is defined from the corresponding Feynman rule in Appendix B.

In the case of h_1 we require that its mass is ≈ 125 GeV and that it is mostly doublet. Besides the usual decay modes for this SM-like Higgs boson, in this model there are two more. These are $h_1 \rightarrow JJ$ and $h_1 \rightarrow JZ$. For the three benchmarks, the branching fractions are $B(h_1 \rightarrow JJ) \approx 3 \times 10^{-5}$ and $B(h_1 \rightarrow JZ) \approx 3 \times 10^{-13}$. We are well within experimental constraints on the Higgs invisible width, as branching fractions bigger than 22% are excluded at 95% CL [27]. These modes are suppressed due to two different reasons. The mode $h_1 \rightarrow JZ$ is suppressed because the Majoron J is mostly singlet. The decay mode $h_1 \rightarrow JJ$ is suppressed because in addition we require a small value for β_2 .

Fig. 8 shows the branching fractions of our light Higgs h_1 . In the top frame we scan the parameters without any restriction, varying λ_1 between $[0, 4]$, in order not to constrain the Higgs mass, as we need to make sure the points

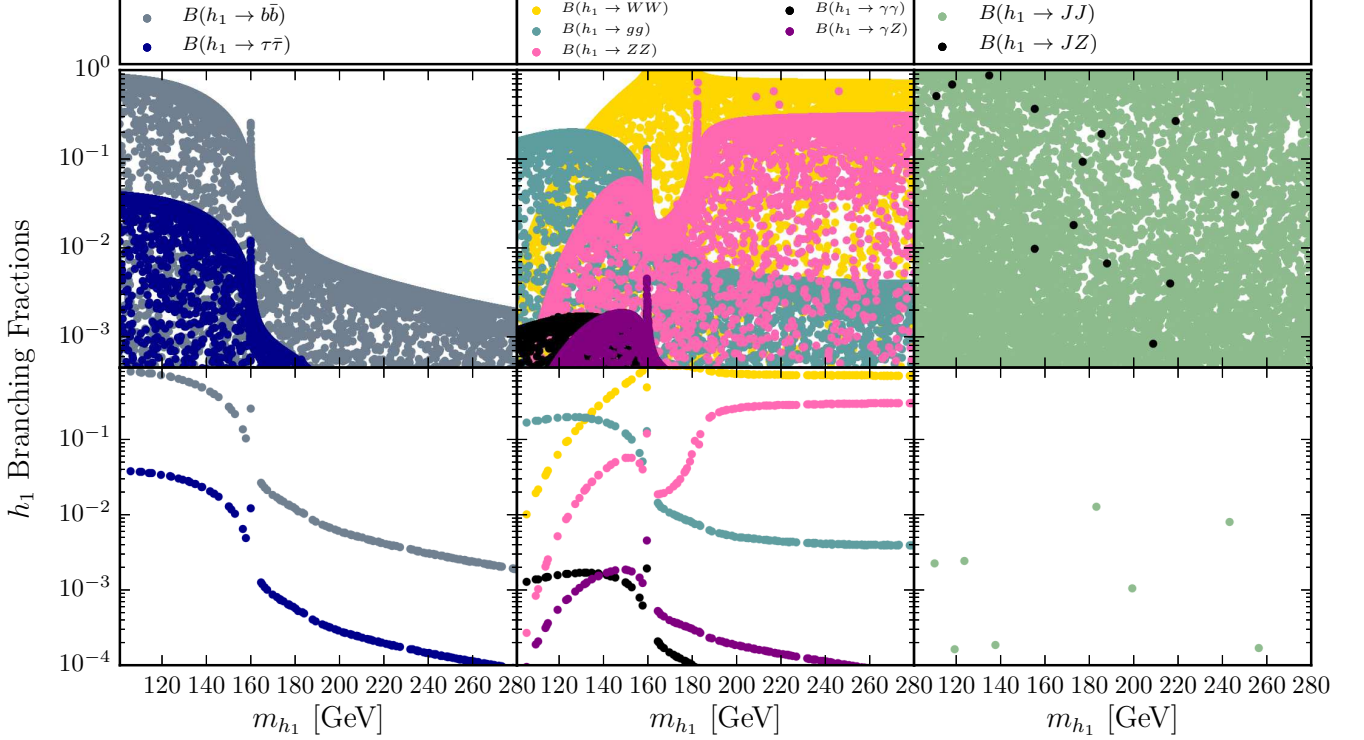


FIG. 8. Branching fractions for the h_1 scalar with (bottom) and without (top) restrictions, as explained in the text.

TABLE VIII. Branching fractions for h_2 in the three different benchmarks.

Branching Fraction	B1	B2	B3
$B(h_2 \rightarrow t\bar{t})$	0.3	7.9×10^{-3}	-
$B(h_2 \rightarrow b\bar{b})$	6.0×10^{-4}	9.5×10^{-6}	3.4×10^{-7}
$B(h_2 \rightarrow \tau\tau)$	3.0×10^{-5}	4.5×10^{-7}	1.6×10^{-8}
$B(h_2 \rightarrow WW)$	7.0×10^{-3}	3.0×10^{-2}	3.6×10^{-6}
$B(h_2 \rightarrow ZZ)$	0.6	1.0×10^{-2}	1.3×10^{-4}
$B(h_2 \rightarrow gg)$	7.2×10^{-3}	1.3×10^{-4}	1.0×10^{-6}
$B(h_2 \rightarrow \gamma\gamma)$	7.7×10^{-6}	2.9×10^{-5}	1.8×10^{-3}
$B(h_2 \rightarrow Z\gamma)$	1.6×10^{-6}	1.6×10^{-7}	1.9×10^{-7}
$B(h_2 \rightarrow JJ)$	1.2×10^{-4}	0.9	0.9
$B(h_2 \rightarrow JZ)$	3.0×10^{-2}	3.6×10^{-12}	2.5×10^{-6}
$B(h_2 \rightarrow h_1 h_1)$	0.1	1.7×10^{-2}	1.0×10^{-6}

in the plot are consistent with a SM-like Higgs. Also is useful to keep the mass free to observe the effect of the constraints and to facilitate the comparison with h_2 . On the top frame β_2 is not constrained and varies between $[-4, 4]$ so we can clearly see the suppression in the Majoron decays once we constrain its value in the bottom frame. The bottom frame includes all constraints from Section III. The branching fractions in our three benchmarks for h_2 are given in Table VIII. We mention first that h_2 has a larger doublet component in B2, and for that reason decay rates to fermions are larger in that benchmark.

Nevertheless, this fact is obscured in branching fractions because the total decay rate is also very different. Similarly, decay rates to gauge bosons are larger in B2, but not necessarily the same is true at the level of branching fractions. Clearly, looking at branching fractions, decays of h_2 to two Majorons (invisible decay) dominate in B2 and B3 because h_2 has a large singlet component in those two benchmarks.

Fig. 9 shows the branching fractions as a function of the scalar mass m_{h_2} , evolving from our three benchmarks, while Fig. 10 shows a scan of the h_2 decays, with all the constraints from Section III implemented.

The curves shown in Fig. 9 confirms the previous observations. These curves are found by keeping the values of the independent parameters as in the 3 different benchmarks, and varying the value of κ in order to keep m_{h_2} free. Since due to mixing this procedure will also vary the value of $m_{h_1} \approx 125$ GeV, we keep λ_1 also free to compensate, as in Table II. We show also as a vertical solid line the value of m_{h_2} in the corresponding benchmark. In the case of B2, near the vertical line h_2 is mainly singlet, and κ affects very little to m_{h_2} . If κ is sufficiently different from its starting value in B2 h_2 becomes mostly triplet. The value for m_{h_2} cannot be larger than its value in the benchmark because by then h_2 is mostly singlet and κ has little effect. Something similar happens with B3. In all cases $h_2 \rightarrow ZZ$ and $h_2 \rightarrow WW$ are important. Decays

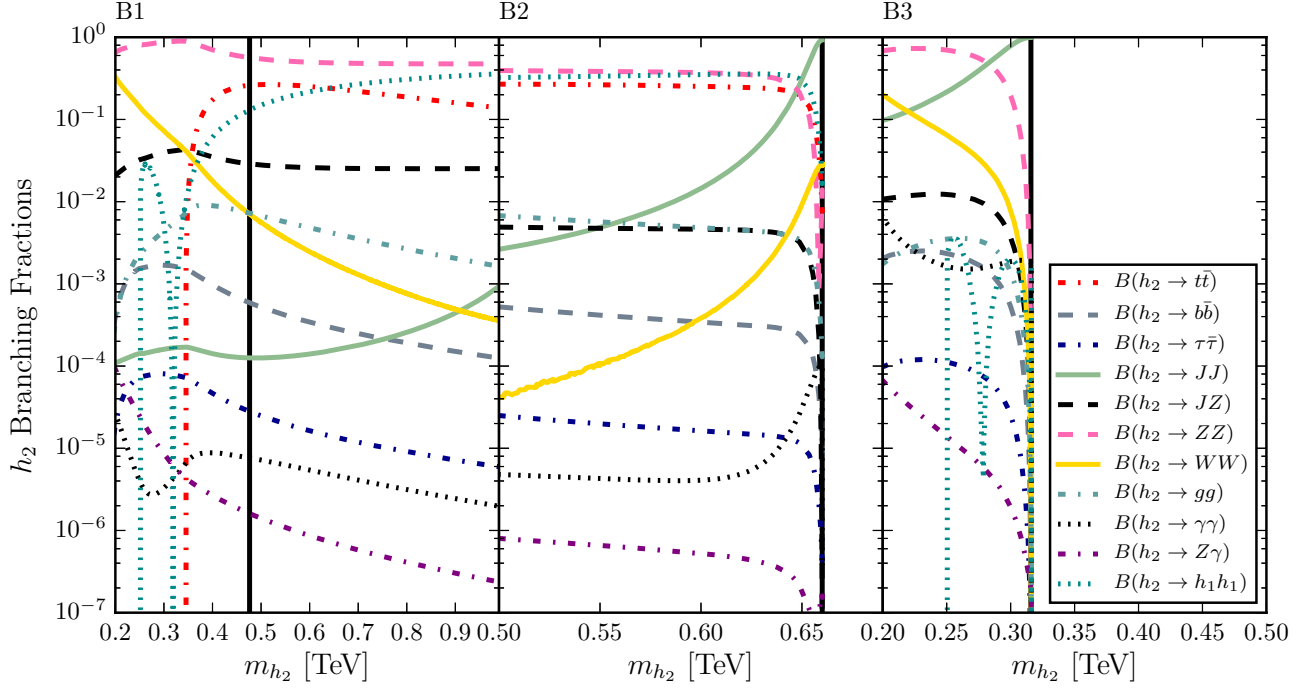


FIG. 9. Branching fractions for the h_2 scalar in the three benchmarks as a function of m_{h_2} . The parameter κ is varied to move m_{h_2} , as explained in the text. The vertical solid line in each frame corresponds to our benchmark point. The plot includes all constrains from Section III.

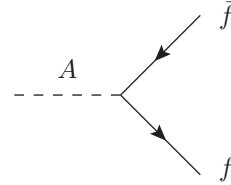
to fermions depend strongly on the (small) h_2 component to doublet. In the scan in Fig. 10, we plot h_2 branching fractions while all the parameters are varied according to Table II. We see that the values of the branching fractions separates in two regions, that we plot separately in the two column plot. These two sectors corresponds to a mainly triplet (left column) or mainly singlet (right column) h_2 . The scan shows that if h_2 is mainly triplet (as in B1) decay modes $h_2 \rightarrow ZZ$ and $h_2 \rightarrow h_1 h_1$ can dominate, with $h_2 \rightarrow JZ$ sometimes also important. On the contrary, if h_2 is mainly singlet (as in B2) the decay mode $h_2 \rightarrow JJ$ dominates by far, with $h_2 \rightarrow WW$ and $h_2 \rightarrow ZZ$ following in importance. The $h_2 \rightarrow t\bar{t}$ branching fractions can be large as long as the other decay rates are also small.

B. A Decays

Now we study the decays of the CP -odd Higgs boson A . The relevant decays at tree-level are to third generation fermions, $A \rightarrow t\bar{t}$, $A \rightarrow b\bar{b}$, $A \rightarrow \tau\tau$, to CP -even Higgs bosons and a Majoron, $A \rightarrow h_i J$, and to CP -even Higgs bosons and a Z gauge boson, $A \rightarrow h_i Z$. We also consider the 1-loop decays to $\gamma\gamma$, $Z\gamma$ and gg for completeness.

The decay of A to fermions, represented by the Feyn-

man diagram,



is given by

$$\Gamma(A \rightarrow f\bar{f}) = \frac{N_c m_A}{8\pi} \left[1 - 4 \frac{m_f^2}{m_A^2} \right]^{\frac{1}{2}} |\lambda_{Aff}|^2, \quad (31)$$

with a coupling

$$\lambda_{Aff} = \frac{1}{\sqrt{2}} O_\varphi^{32} h_f, \quad (32)$$

as seen in Appendix B. h_f is the Yukawa coupling of the fermion. Since A is always mainly triplet, O_φ^{32} is always small. The decay $A \rightarrow f\bar{f}$ proceeds just because the A eigenfunction has a small component of doublet, as indicated in eq. (A5).

The A boson can also decay into a CP -even Higgs and a Z boson. The corresponding Feynman diagram is,

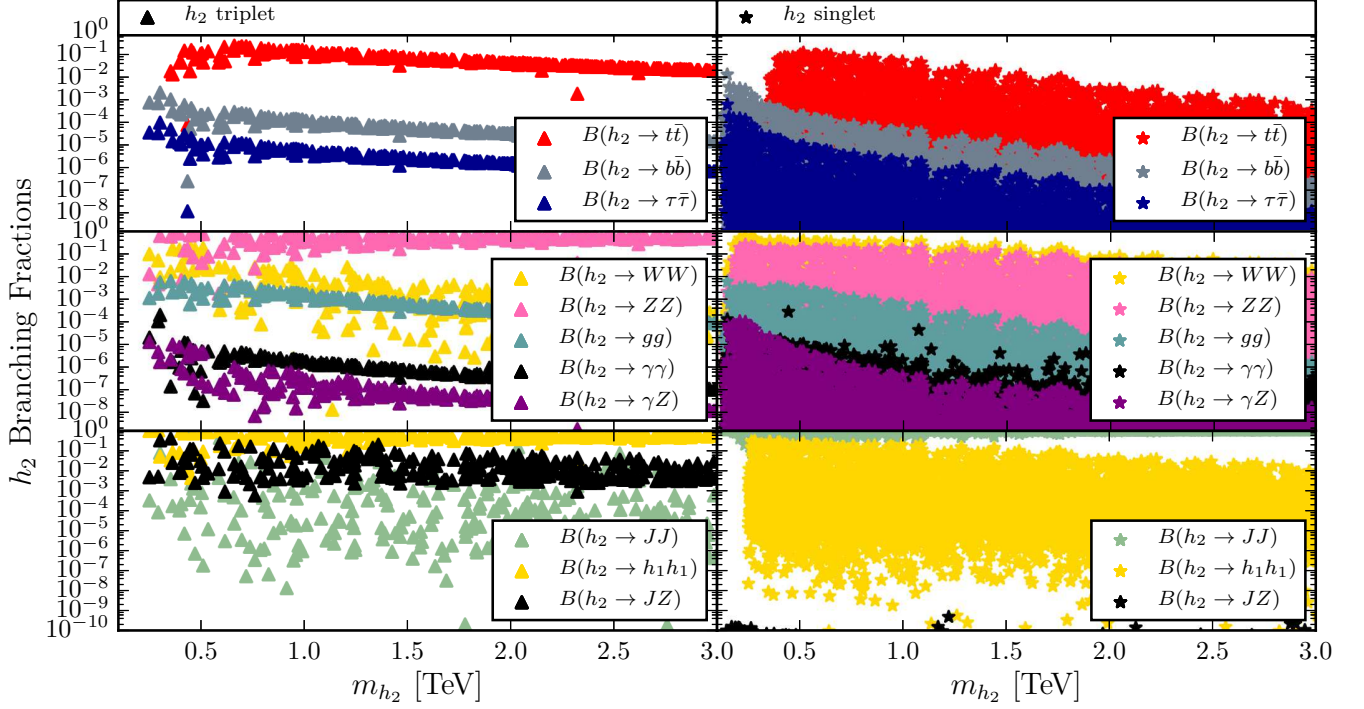


FIG. 10. Branching fractions for the h_2 scalar as a function of m_{h_2} . The left column shows points where h_2 is triplet-like (i.e. $|O_\chi^{23}| > 0.95$). The right column shows points where h_2 is singlet-like (i.e. $|O_\chi^{21}| > 0.95$). Parameters are varied according to Table II. The scan includes all constraints from Section III.

similar for B1 and B2, the difference is due to the value of m_A .

The decay to a CP -even Higgs boson and a Majoron is represented by the following Feynman diagram,



The decay rate is given by the formula,

$$\Gamma(A \rightarrow h_i Z) = \frac{\lambda_{Ah_i Z}^2 m_A^3}{16\pi m_Z^2} \lambda^{3/2}(1, m_{h_i}^2/m_A^2, m_Z^2/m_A^2), \quad (33)$$

with a coupling

$$\lambda_{Ah_i Z} = \frac{g}{2c_W} (O_\chi^{i2} O_\varphi^{32} - 2O_\chi^{i3} O_\varphi^{33}), \quad (34)$$

as seen in Appendix B. The λ function is defined in eq. (13). In the case $A \rightarrow h_2 Z$, since A is always mainly triplet, there is no phase space in B1, where h_2 is also a triplet and has a mass almost equal to the mass of A . In the case $A \rightarrow h_1 Z$, since the couplings are more or less

The decay rate is

$$\Gamma(A \rightarrow h_i J) = \frac{M_{h_i a_1 a_2}^2}{16\pi m_A} \lambda^{1/2}(1, m_{h_i}^2/m_A^2, m_J^2/m_A^2), \quad (35)$$

with the coupling $M_{h_i a_1 a_2}$ (with units of mass) given in Appendix B.

The decay to $\gamma\gamma$ is given by [34]

$$\Gamma(A \rightarrow \gamma\gamma) = \frac{\alpha^2 g^2 m_A^2}{1024\pi^3 m_W^2} \left| \frac{4\sqrt{2}}{3h_t} F_{1/2}(\tau_t) \lambda_{Att} \right|^2 \quad (36)$$

with $\tau_t = 4m_t^2/m_A^2$ and the $F_{1/2}$ function for a pseudoscalar is defined in Appendix C of Ref. [34].

The decay to $Z\gamma$ is given by [34]

$$\Gamma(A \rightarrow Z\gamma) = \frac{\alpha g^2}{2048\pi^4 m_W^4} |A_t|^2 m_A^3 \left(1 - \frac{m_Z^2}{m_A^2}\right)^3, \quad (37)$$

where A_t is defined in equation 23 (replacing h with A). Finally, the decay to two gluons is [34]

$$\Gamma(A \rightarrow gg) = \frac{\alpha_s^2 g^2 m_A^3}{128\pi^3 m_W^2} \left| \frac{4\sqrt{2}}{3h_t} F_{1/2}(\tau_t) \lambda_{Att} \right|^2. \quad (38)$$

Branching fractions for the decay of A for our three benchmarks are given in Table IX. The A boson compo-

TABLE IX. Branching fractions for A in our three different benchmarks.

Branching Fraction	B1	B2	B3
$B(A \rightarrow tt)$	0.5	0.2	-
$B(A \rightarrow b\bar{b})$	5.5×10^{-4}	1.5×10^{-4}	6.0×10^{-3}
$B(A \rightarrow \tau\tau)$	2.6×10^{-5}	7.0×10^{-6}	2.8×10^{-4}
$B(A \rightarrow h_1 Z)$	0.5	0.8	0.9
$B(A \rightarrow h_1 J)$	1.7×10^{-2}	4.4×10^{-3}	2.0×10^{-2}
$B(A \rightarrow h_2 Z)$	-	5.0×10^{-2}	-
$B(A \rightarrow h_2 J)$	-	1.1×10^{-4}	-
$B(A \rightarrow gg)$	1.4×10^{-2}	2.7×10^{-3}	6.2×10^{-2}
$B(A \rightarrow \gamma\gamma)$	1.7×10^{-5}	3.4×10^{-6}	7.7×10^{-5}
$B(A \rightarrow Z\gamma)$	8.2×10^{-7}	2.6×10^{-7}	2.0×10^{-6}

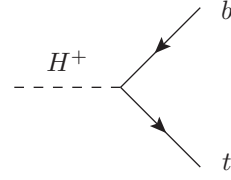
nent to doublet is the same for B1 and B2, but m_A is not. This leads to larger decay rates to fermions in B2. Since the total decay rate is also different, this is not observed for branching fractions and in fact, the opposite happens. Note that in B1 and B3 the decays of A to h_2 and a J or a Z are not kinematically allowed. The same happens in B3 for the decay to top quarks. In B2, A can be much heavier than h_2 thus, the decay $A \rightarrow h_2 Z$ is open.

Fig. 11 shows the branching fractions of A as a function of its mass. The curves are obtained starting from each of the 3 benchmarks and vary κ to change m_A . Since this procedure will also change m_{h_1} , which we want fixed to 125 GeV, we change also the value of λ_1 to recover $m_{h_1} \approx 125$ GeV, as in Table II. In all cases, the modes $A \rightarrow h_1 Z$ and $A \rightarrow t\bar{t}$ dominate. In B3 the decay mode $A \rightarrow h_2 Z$ is open and can be relevant too.

Fig. 12 shows a general scan where all the parameters are varied according to Table II. It shows that the decay mode $A \rightarrow h_1 Z$ dominates. If the channel is open, when h_2 is mainly singlet, the decay channel $A \rightarrow h_2 Z$ is also very important.

C. H^\pm Decays

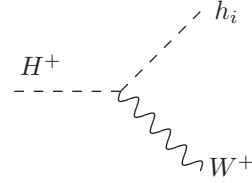
In this Section we study tree-level decays of the singly charged Higgs boson. The decay to $t\bar{b}$, represented by the Feynman diagram,



has a rate

$$\Gamma(H^\pm \rightarrow t\bar{b}) = \frac{N_c (O_+^{21})^2}{16\pi m_{H^\pm}^3} \left[(h_t^2 + h_b^2)(m_{H^\pm}^2 - m_t^2 - m_b^2) - 4h_t h_b m_t m_b \right] \lambda^{1/2}(m_{H^\pm}^2, m_t^2, m_b^2). \quad (39)$$

Similarly, the decay $H^\pm \rightarrow h_i W^\pm$



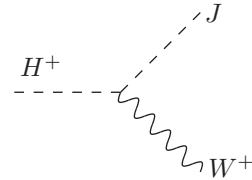
has a rate given by

$$\Gamma(H^\pm \rightarrow h_i W^\pm) = \frac{g^2 |\lambda_{H^\pm h_i W^\pm}|^2}{64\pi m_{H^\pm}^3 m_W^2} \lambda^{3/2}(m_{H^\pm}^2, m_{h_i}^2, m_W^2), \quad (40)$$

with,

$$\lambda_{H^\pm h_i W^\pm} = O_+^{21} O_\chi^{i2} - \sqrt{2} O_+^{22} O_\chi^{i3}. \quad (41)$$

The decay to a Majoron and a W^\pm boson is



with a decay rate,

$$\Gamma(H^\pm \rightarrow JW^\pm) = \frac{g^2 |\lambda_{H^\pm JW^\pm}|^2}{64\pi m_{H^\pm}^3 m_W^2} [m_{H^\pm}^2 - m_W^2]^3, \quad (42)$$

where

$$\lambda_{H^\pm JW^\pm} = O_+^{21} O_\varphi^{22} + \sqrt{2} O_+^{22} O_\varphi^{23}, \quad (43)$$

To finish, the decay to a Z and a W^\pm boson is,

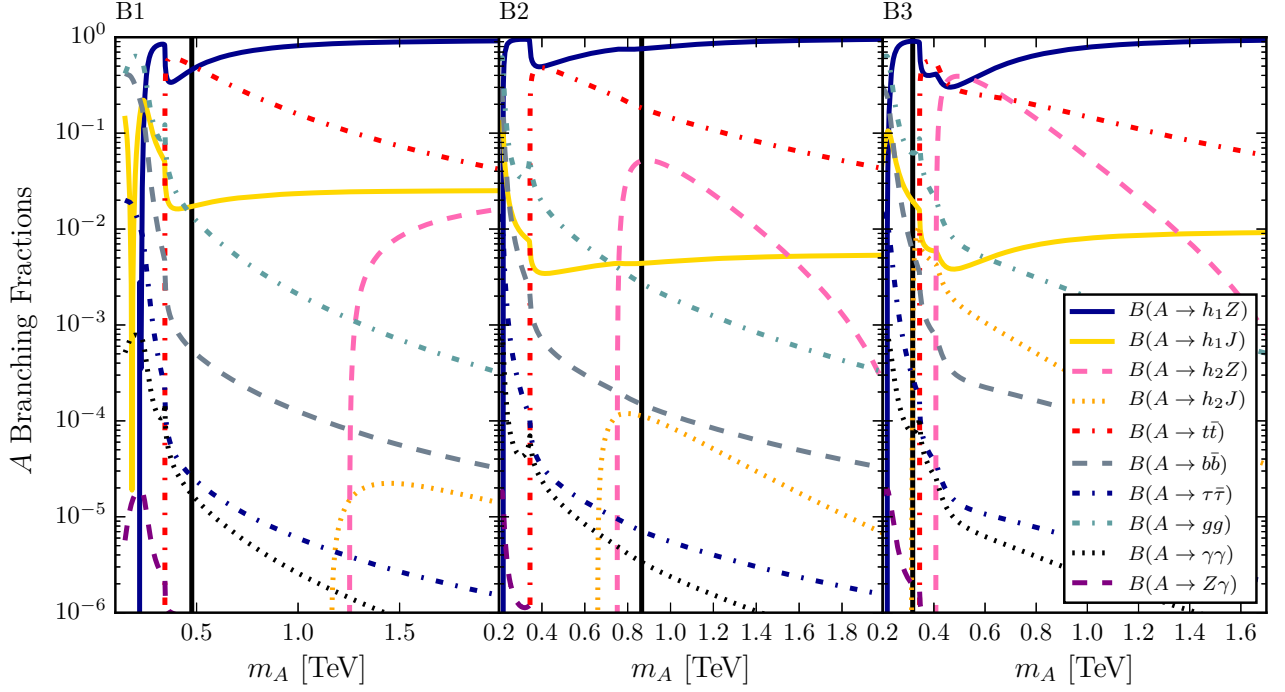
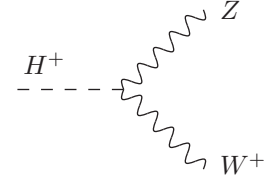


FIG. 11. CP -odd Higgs A branching fractions in the three benchmarks as a function of m_A . The parameter κ is varied to move m_A , as explained in the text. The vertical solid line in each frame corresponds to our benchmark point. The plot includes all constrains from Section III.



and has the following decay rate

$$\Gamma(H^\pm \rightarrow ZW^\pm) = \frac{g^4 |M_{H^\pm ZW^\mp}|^2}{256\pi m_W^4 m_{H^\pm}^3} \left[m_{H^\pm}^4 + m_Z^4 + 10m_Z^2 m_W^2 + m_W^4 - 2m_{H^\pm}^2 (m_W^2 + m_Z^2) \right] \lambda^{1/2}(m_{H^\pm}^2, m_Z^2, m_W^2), \quad (44)$$

with

$$M_{H^\pm ZW^\mp} = O_+^{21} s_W v_\phi - \sqrt{2} O_+^{22} (1 + s_W^2) v_\Delta. \quad (45)$$

In Table X we show the singly charged Higgs branching

fractions in our three benchmarks. Note that the decay $H^\pm \rightarrow h_2 W^\pm$ is not kinematically allowed in B1 and B3. Branching fractions of $H^\pm \rightarrow h_1 W^\pm$ are dominant in the three benchmarks.

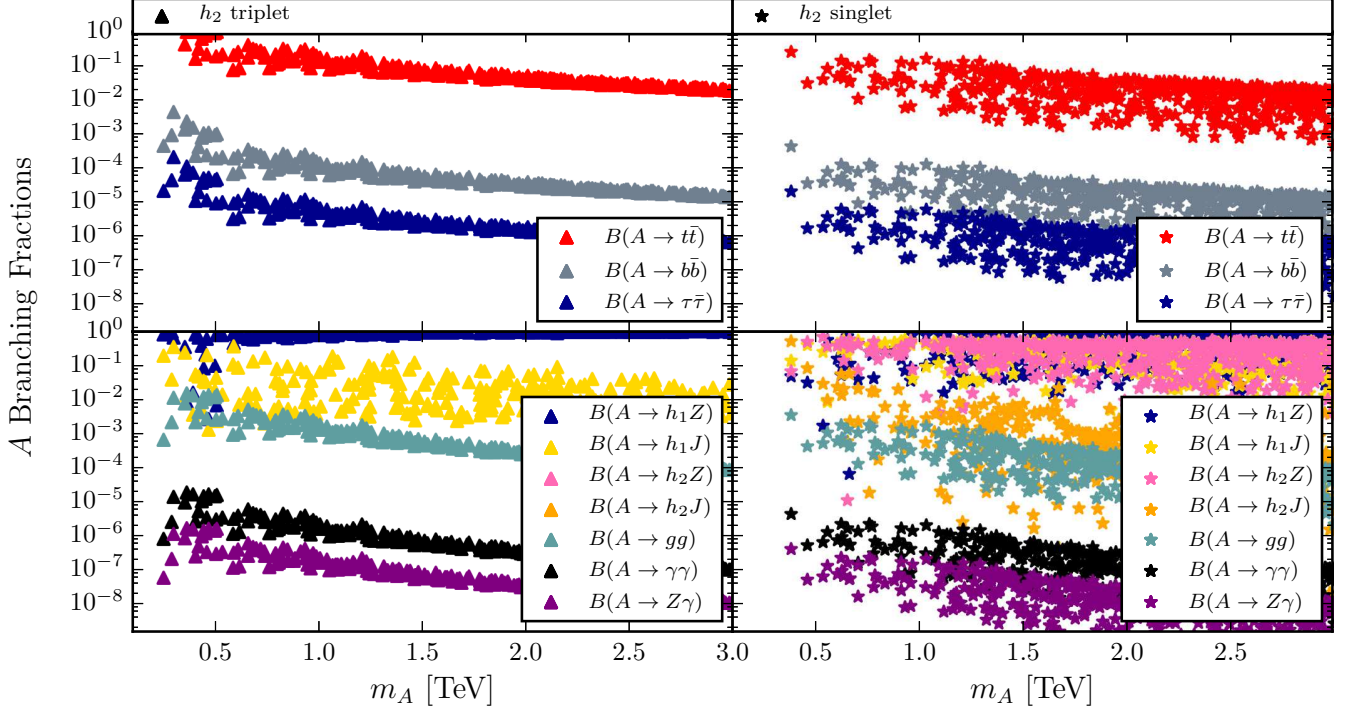


FIG. 12. Branching fractions for the A scalar as a function of m_A . The left column shows points where h_2 is triplet-like (i.e. $|O_X^{23}| > 0.95$). The right column shows points where h_2 is singlet-like (i.e. $|O_X^{21}| > 0.95$). Parameters are varied according to Table II. The scan includes all constrains from Section III.

TABLE X. Branching fractions for H^\pm in our three benchmarks.

Branching Fraction	B1	B2	B3
$B(H^\pm \rightarrow tb)$	7.0×10^{-2}	2.0×10^{-2}	0.2
$B(H^\pm \rightarrow h_1 W^\pm)$	0.7	0.8	0.6
$B(H^\pm \rightarrow h_2 W^\pm)$	-	5.7×10^{-3}	-
$B(H^\pm \rightarrow JW^\pm)$	3.0×10^{-3}	5.1×10^{-4}	1.6×10^{-3}
$B(H^\pm \rightarrow ZW^\pm)$	0.2	0.2	0.3

Fig. 13 shows the branching fractions of H^\pm as a function of its mass. The curves are obtained starting from each of the 3 benchmarks and vary κ according to Table II to change the value of m_H^\pm . λ_1 also varies as in Table II to recover $m_{h_1} \approx 125$ GeV.

Fig. 14 shows the H^\pm branching fractions as a function of its mass in a general scan. Decays to $h_1 W^\pm$ dominate, independent of the composition of h_2 . Decays to ZW^\pm follow in importance. Also important are decays to $h_2 W^\pm$, when h_2 is singlet-like, as when h_2 is triplet-like, its mass is very close to the mass of m_{H^\pm} (as in B1), so there is no phase space for the decay in this case.

VII. PROMISING CHANNELS FOR h_2 , A AND H^\pm

We now briefly comment on the most promising channels for discovery of h_2 , A and H^\pm at future e^+e^- colliders.

A promising channel for the discovery of h_2 , given its large cross-section as discussed in Section V A, is $e^+e^- \rightarrow h_2 tt$. Thinking of B1, the largest decays fractions for h_2 are to ZZ as shown in Table VIII. Considering leptonic decays of the W and Z , the signal is

$$e^+e^- \rightarrow ZZt\bar{t} \rightarrow l^+l^-l^+l^-l^+\nu_l l^-\nu_l b\bar{b} \quad (46)$$

with $l = e, \mu$. The signal contains 2 b -jets + 6 leptons + p_T^{miss} (missing transverse momenta). For B1 at $\sqrt{s} = 1$ TeV, the cross-section is estimated as

$$\begin{aligned} \sigma_{2b6lp_T^{\text{miss}}} &\approx \sigma(e^+e^- \rightarrow h_2 t\bar{t}) \times B(h_2 \rightarrow ZZ) \\ &\quad \times B(Z \rightarrow l^+l^-)^2 \times B(W^\pm \rightarrow l^\pm \nu)^2 \\ &\approx 3 \times 10^{-5} \text{ fb} \end{aligned} \quad (47)$$

resulting in less than one event to be discoverable with $\mathcal{L} = 1000 \text{ fb}^{-1}$, so too little to be observed unfortunately. Possible SM backgrounds to this signature include $e^+e^- \rightarrow ZZZ$ and $e^+e^- \rightarrow ZZt\bar{t}$. Multi-lepton

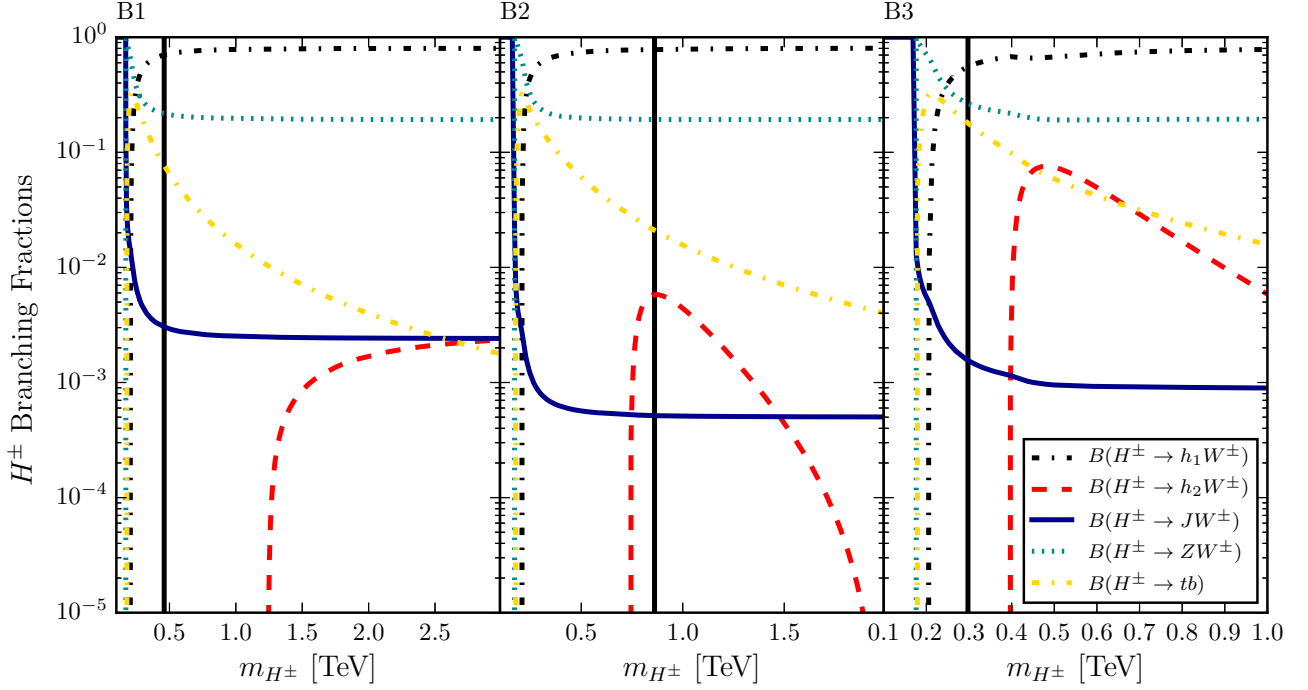


FIG. 13. Branching fraction for the H^\pm scalar in the three benchmarks as a function of m_{H^\pm} . The parameter κ is varied to move m_{H^\pm} , as explained in the text. The vertical solid line in each frame corresponds to our benchmark point. The plot includes all constrains from Section III.

signatures in the “23” HTM were studied in the context of the LHC in Refs. [19, 36], where it was shown that after requiring kinematic cuts in the transverse momenta of the leptons, signatures with 6 leptons have no background, even though the signal is also scarce. Therefore, multi-lepton signatures are relevant for higher integrated luminosities. We could require similar leptonic kinematic cuts in the case of e^+e^- , in addition of requiring 2 b -tagged jets and small p_T^{miss} due to the two neutrinos.

For B2 the decay $h_2 \rightarrow JJ$ dominates. If one W boson decays hadronically and the other leptonically, then we will have a 4 b -jets + p_T^{miss} signature, assuming the lepton escapes undetected. This channel was studied in detail in Ref. [11] for our “123” model, where it was shown that with appropriate cuts in p_T^{miss} , number of jets and invariant mass distributions the background is removed while keeping high signal efficiency.

In the case of the CP -odd Higgs A , there are two relevant processes. $e^+e^- \rightarrow AZZ$ has the highest cross-section for B1 and B2. In the case where $A \rightarrow t\bar{t}$ we have the same signature as before for h_2 . The decay $A \rightarrow h_1Z$ also dominates in our benchmarks. The dominant decay $h_1 \rightarrow b\bar{b}$ follows, leading to topologies with leptons and b -jets (with no missing transverse momenta), depending on the decay of the Z . The cross-section for,

$$e^+e^- \rightarrow AZZ \rightarrow h_1ZZZ \rightarrow b\bar{b}l^+l^-l^+l^- \quad (48)$$

leads to a 2 b -jet+6 leptons signature. The cross-section for B1 at $\sqrt{s} = 1$ TeV is estimated as,

$$\begin{aligned} \sigma_{2b6l} &\approx \sigma(e^+e^- \rightarrow AZZ) \times B(A \rightarrow h_1Z) \times B(h_1 \rightarrow b\bar{b}) \\ &\times B(Z \rightarrow l^+l^-)^3 \\ &\approx 1.0 \times 10^{-4} \text{ fb} \end{aligned} \quad (49)$$

resulting in less than one event with $\mathcal{L} = 1000 \text{ fb}^{-1}$. Possible backgrounds are very similar and include the ones in equation 47, so similar cuts can be applied to suppress them.

The associated production $e^+e^- \rightarrow AJJ$ dominates in B3 with $A \rightarrow b\bar{b}$, leading to the topology of 2 b -jets + p_T^{miss} . This signal was studied for the “23” HTM in [37], with largest background coming from $e^+e^- \rightarrow W^+W^-$ and $e^+e^- \rightarrow ZZ$. The authors concluded that the most efficient way to improve the signal-to-background ratio is to require b -tagged jets and large p_T^{miss} , in addition to charged multiplicity and an invariant mass cut close to the mass of the visibly decaying particle.

Production for the singly charged Higgs dominates in $e^+e^- \rightarrow H^+H^- \rightarrow H^+h_1W^-$ for most of our benchmarks (see Figure 6). This is followed by the decay of

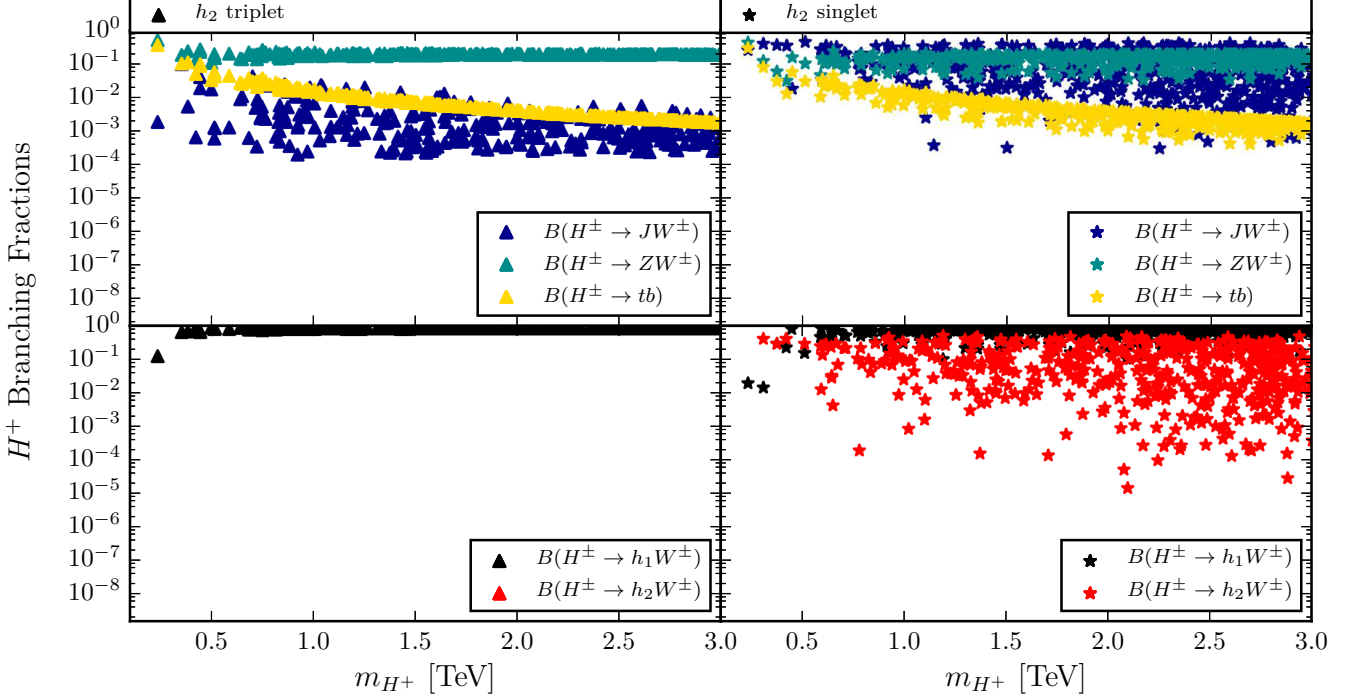


FIG. 14. Branching fractions for the H^+ scalar as a function of m_{H^+} . The left column shows points where h_2 is triplet-like (i.e. $O_\chi^{21} > 0.95$). The right column shows points where h_2 is singlet-like (i.e. $O_\chi^{23} > 0.95$). Parameters are varied according to Table II. The scan includes all constrains from Section III.

$H^+ \rightarrow h_1 W^+$, which has the highest branching fraction (see Table X). An optimal discovery channel would be when $h_1 \rightarrow b\bar{b}$ and when one W boson decays hadronically and the other leptonically,

$$e^+e^- \rightarrow H^+ h_1 W^- \rightarrow h_1 W^+ h_1 W^- \rightarrow b\bar{b} l^\pm \nu_l b\bar{b} q\bar{q} \quad (50)$$

resulting in an event topology of $4b$ -jets + 2 jets + 1 lepton + p_T^{miss} , where the lepton $l = e, \mu$. This distinctive signature was studied for a charged Higgs in the context of Two-Higgs doublet models [38, 39]. The mass of the singly charged Higgs can be reconstructed and the events can be selected with b -tagging techniques, in addition to requiring one isolated lepton. Also, two jets must have the W mass.

We can estimate the visible cross-section for this final state. For $\sqrt{s} = 1$ TeV in B1 we have,

$$\begin{aligned} \sigma_{4bp_T^{\text{miss}}ljj} &\approx \sigma(e^+e^- \rightarrow H^+ h_1 W^-) \\ &\times B(H^+ \rightarrow h_1 W^+) \times B(h_1 \rightarrow b\bar{b})^2 \\ &\times B(W^\pm \rightarrow l^\pm \nu_l) \times B(W^\pm \rightarrow q\bar{q}) \\ &\approx 0.04 \text{ fb} \end{aligned} \quad (51)$$

and since the ILC has a yearly integrated luminosity of 1000 fb^{-1} , this results in about 40 potentially discoverable events. A relevant SM background for this signature

is the process $e^+e^- \rightarrow t\bar{t}b\bar{b}$. Our estimation yields a visible cross-section of $\sigma_{\text{SM-}4bp_T^{\text{miss}}ljj} \approx 0.4 \text{ fb}$, which is quite significant. The signal-to-background ratio can be enhanced by applying the selection cuts above mentioned. It was also shown in Ref. [38] that one can suppress this big irreducible background to a negligible level by using a technique that allows the reconstruct of the neutrino four-momentum.

Of course a more detailed simulation study should be done in order to suppress backgrounds further and improve signal efficiency for the channels mentioned. A fully fledged study in this direction, considering also detector efficiencies, goes beyond the scope of this paper and we leave it for a future work.

VIII. CONCLUSIONS

We have studied the Higgs phenomenology of a model with a scalar triplet, a scalar singlet and a scalar doublet under $SU(2)$. In this “123” variant of the Higgs triplet model the singlet acquires a vacuum expectation value, which spontaneously breaks lepton number. The vacuum expectation value generated for the triplet provides a mass term for neutrinos. This feature makes it a well motivated model to look for at particle colliders.

The lightest CP -even Higgs, h_1 , has been identified

with the SM-like Higgs boson discovered at the LHC, which constrains the parameters in the scalar potential of the model. We studied the production cross-sections and decay ratios of the second heaviest CP -even Higgs h_2 , the CP -odd Higgs A and the singly charged Higgs H^\pm . We found that production cross-sections at hadron colliders can be very low for these states, so we perform a numerical analysis assessing the discovery potential at future lepton colliders.

We find characteristic features in cases where h_2 is singlet-like, triplet-like or a mixture. The main 2-body production mode for h_2 is associated production with a CP -odd state A . We note that cross-sections for A and H^\pm are enhanced when a second heavy particle is also produced on-shell. Invisible decays of h_2 to Majorons can be very important. Decays of the singly charged Higgs $H^\pm \rightarrow h_1 W^\pm$ dominate. These features lead to promising channels for discovery of h_2 and A , in particular in the $4b$ -jets+ p_T^{miss} and $2b$ -jets+ p_T^{miss} final states, as shown in Ref. [11] and Ref. [37], respectively, as we estimate the most promising signal with leptons in the final state are too small to be observed. The $4b$ -jets + 2 jets + 1 lepton + p_T^{miss} final state is optimal for the discovery of the singly charged Higgs. These signals provides a test of the “123” HTM at future e^+e^- colliders.

ACKNOWLEDGMENTS

SB was funded by the PUC Vice Rectorcy of Research Scholarship. The work of MAD was supported by Fondecyt 1141190. The work of BK was supported by Fondecyt 1161150. GC was funded by the postgraduate Conicyt-Chile/Cambridge Trusts Scholarship 84130011 and also acknowledges partial support from STFC grant ST/L000385/1.

Appendix A: Convention for Diagonalization.

The diagonalization in the charged scalar sector is,

$$\begin{bmatrix} h_1^+ \\ h_2^+ \end{bmatrix} \equiv \begin{bmatrix} G^+ \\ H^+ \end{bmatrix} = O_+ \begin{bmatrix} \phi^{*-} \\ \Delta^+ \end{bmatrix} \equiv \begin{pmatrix} -c_\beta & s_\beta \\ s_\beta & c_\beta \end{pmatrix} \begin{bmatrix} \phi^{*-} \\ \Delta^+ \end{bmatrix} \quad (\text{A1})$$

and the diagonalization in the neutral scalar sector proceeds as,

$$\begin{bmatrix} h_1 \\ h_2 \\ h_3 \end{bmatrix} = O_\chi \begin{bmatrix} \chi_\sigma \\ \chi_\phi \\ \chi_\Delta \end{bmatrix}, \quad \begin{bmatrix} a_1 \\ a_2 \\ a_3 \end{bmatrix} \equiv \begin{bmatrix} G^0 \\ J \\ A \end{bmatrix} = O_\varphi \begin{bmatrix} \varphi_\sigma \\ \varphi_\phi \\ \varphi_\Delta \end{bmatrix}, \quad (\text{A2})$$

where O_χ and O_φ are 3×3 matrices.

The mass matrix in eq. (4) is diagonalized by the matrix,

$$O_\varphi = \begin{bmatrix} 0 & \frac{1}{N_G} & -\frac{2}{N_G} \frac{v_\Delta}{v_\phi} \\ \frac{N_G^2}{N_J} & -\frac{2}{N_J} \frac{v_\Delta^2}{v_\phi v_\sigma} & -\frac{1}{N_J} \frac{v_\Delta}{v_\sigma} \\ \frac{1}{N_A} \frac{v_\Delta}{v_\sigma} & \frac{2}{N_A} \frac{v_\Delta}{v_\phi} & \frac{1}{N_A} \end{bmatrix}, \quad (\text{A3})$$

where

$$\begin{aligned} N_G &= \sqrt{1 + 4 \frac{v_\Delta^2}{v_\phi^2}}, \\ N_J &= \sqrt{N_G^4 + 4 \frac{v_\Delta^4}{v_\phi^2 v_\sigma^2} + \frac{v_\Delta^2}{v_\sigma^2}}, \\ N_A &= \sqrt{1 + 4 \frac{v_\Delta^2}{v_\phi^2} + \frac{v_\Delta^2}{v_\sigma^2}}. \end{aligned} \quad (\text{A4})$$

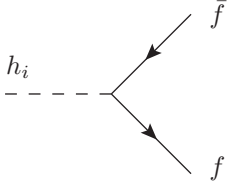
The mass eigenstate fields are,

$$\begin{aligned} G^0 &= \frac{1}{N_G} \varphi_\phi - \frac{2}{N_G} \frac{v_\Delta}{v_\phi} \varphi_\Delta, \\ J &= \frac{N_G^2}{N_J} \varphi_\sigma - \frac{2}{N_J} \frac{v_\Delta^2}{v_\phi v_\sigma} \varphi_\phi - \frac{1}{N_J} \frac{v_\Delta}{v_\sigma} \varphi_\Delta, \\ A &= \frac{1}{N_A} \frac{v_\Delta}{v_\sigma} \varphi_\sigma + \frac{2}{N_A} \frac{v_\Delta}{v_\phi} \varphi_\phi + \frac{1}{N_A} \varphi_\Delta. \end{aligned} \quad (\text{A5})$$

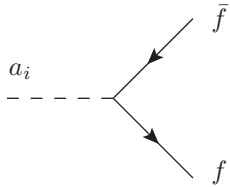
From here we conclude that the Majoron has the tendency to be mainly singlet and that the neutral Goldstone boson has no singlet component (the singlet does not couple to the Z boson).

Appendix B: Feynman Rules.

1. One scalar and two fermions

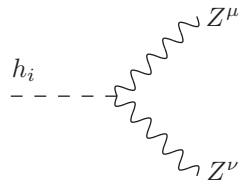


$$= -i O_\chi^{i2} \frac{h_f}{\sqrt{2}}$$



$$= O_\varphi^{i2} \frac{h_f}{\sqrt{2}} \gamma_5$$

2. One scalar and two gauge bosons



$$= i \frac{1}{2} (g^2 + g'^2) (O_\chi^{i2} v_\phi + 4 O_\chi^{i3} v_\Delta) g^{\mu\nu}$$

$$= i\frac{g^2}{2}(O_\chi^{i2}v_\phi + 2O_\chi^{i3}v_\Delta)g_{\mu\nu}$$

$$= -ie(p+p')_\mu\delta_{ij}$$

$$= -2ie(p+p')_\mu$$

3. Two scalars and one gauge boson

$$= \frac{g}{2c_W}(O_\chi^{i2}O_\phi^{j2} - 2O_\chi^{i3}O_\phi^{j3})(p+p')_\mu$$

$$= i\frac{g}{2}(O_+^{i1}O_\chi^{j2} - \sqrt{2}O_+^{i2}O_\chi^{j3})(p+p')_\mu$$

$$= -\frac{ig}{2c_W}\left[O_+^{i1}O_+^{j1}(c_W^2 - s_W^2) - 2O_+^{i2}O_+^{j2}s_W^2\right](p+p')_\mu$$

$$= i\frac{g}{2}(O_+^{i1}O_\chi^{j2} + \sqrt{2}O_+^{i2}O_\chi^{j3})(p+p')_\mu$$

$$= -\frac{ig}{c_W}(c_W^2 - s_W^2)(p+p')_\mu$$

4. Three Scalars

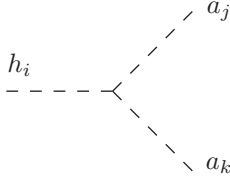
For the case with one CP -even and two CP -odd Higgs bosons, the relevant term in the Lagrangian is

$$\mathcal{L}_{h_i a_j a_k} = M_{h_i a_j a_k} h_i a_j a_k, \quad (\text{B1})$$

where we sum over i, j, k . The coupling $M_{h_i a_j a_k}$ (with units of mass), after symmetrization in j and k is given by the expression

$$\begin{aligned}
M_{h_i a_j a_k} = & -\lambda_1 v_\phi O_\chi^{i2} O_\phi^{j2} O_\phi^{k2} - (\lambda_2 + \lambda_4) v_\Delta O_\chi^{i3} O_\phi^{j3} O_\phi^{k3} - \frac{1}{2} (\lambda_3 + \lambda_5) v_\phi O_\chi^{i2} O_\phi^{j3} O_\phi^{k3} \\
& - \frac{1}{2} [(\lambda_3 + \lambda_5) v_\Delta + \kappa v_\sigma] O_\chi^{i3} O_\phi^{j2} O_\phi^{k2} - \beta_1 v_\sigma O_\chi^{i1} O_\phi^{j1} O_\phi^{k1} - \frac{1}{2} \beta_2 v_\phi O_\chi^{i2} O_\phi^{j1} O_\phi^{k1} \\
& - \frac{1}{2} (\beta_2 v_\sigma + \kappa v_\Delta) O_\chi^{i1} O_\phi^{j2} O_\phi^{k2} - \frac{1}{2} \beta_3 v_\Delta O_\chi^{i3} O_\phi^{j1} O_\phi^{k1} - \frac{1}{2} \beta_3 v_\sigma O_\chi^{i1} O_\phi^{j3} O_\phi^{k3} \\
& - \frac{1}{2} \kappa v_\phi O_\chi^{i2} (O_\phi^{j1} O_\phi^{k3} + O_\phi^{k1} O_\phi^{j3}) - \frac{1}{2} \kappa v_\phi O_\chi^{i3} (O_\phi^{j1} O_\phi^{k2} + O_\phi^{k1} O_\phi^{j2}) - \frac{1}{2} \kappa v_\phi O_\chi^{i1} (O_\phi^{j2} O_\phi^{k3} + O_\phi^{k2} O_\phi^{j3}) \\
& - \frac{1}{2} \kappa v_\Delta O_\chi^{i2} (O_\phi^{j1} O_\phi^{k2} + O_\phi^{k1} O_\phi^{j2}) - \frac{1}{2} \kappa v_\sigma O_\chi^{i2} (O_\phi^{j2} O_\phi^{k3} + O_\phi^{k2} O_\phi^{j3}). \tag{B2}
\end{aligned}$$

This leads to the following Feynman rule,



$$= iM_{h_i a_j a_k} \text{ (twice larger if } j = k\text{)}.$$

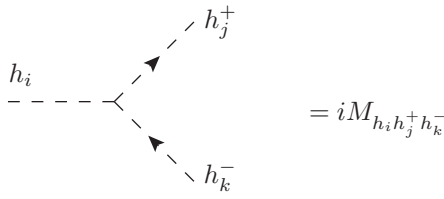
For one CP -even and two charged Higgs bosons, the relevant term in the Lagrangian is,

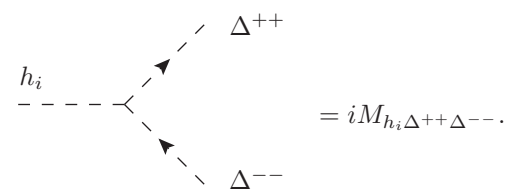
$$\mathcal{L}_{h_i h_j^+ h_k^-} = M_{h_i h_j^+ h_k^-} h_i h_j^+ h_k^- \tag{B3}$$

where we sum over i, j, k . The coupling $M_{h_i h_j^+ h_k^-}$ (with units of mass) is given by the expression

$$\begin{aligned}
M_{h_i h_j^+ h_k^-} = & -2\lambda_1 v_\phi O_\chi^{i2} O_+^{j1} O_+^{k1} - 2(\lambda_2 + \lambda_4) v_\Delta O_\chi^{i3} O_+^{j2} O_+^{k2} - (\lambda_3 + \frac{1}{2}\lambda_5) v_\phi O_\chi^{i2} O_+^{j2} O_+^{k2} \\
& - \lambda_3 v_\Delta O_\chi^{i3} O_+^{j1} O_+^{k1} - \frac{1}{2\sqrt{2}} \lambda_5 v_\phi O_\chi^{i3} O_+^{j2} O_+^{k1} - \frac{1}{2\sqrt{2}} \lambda_5 v_\phi O_\chi^{i3} O_+^{j1} O_+^{k2} \\
& - \frac{1}{\sqrt{2}} (\frac{1}{2}\lambda_5 v_\Delta - \kappa v_\sigma) O_\chi^{i2} O_+^{j2} O_+^{k1} - \frac{1}{\sqrt{2}} (\frac{1}{2}\lambda_5 v_\Delta - \kappa v_\sigma) O_\chi^{i2} O_+^{j1} O_+^{k2} - \beta_2 v_\sigma O_\chi^{i1} O_+^{j1} O_+^{k1} \\
& - \beta_3 v_\sigma O_\chi^{i1} O_+^{j2} O_+^{k2} + \frac{1}{\sqrt{2}} \kappa v_\phi O_\chi^{i1} O_+^{j2} O_+^{k1} + \frac{1}{\sqrt{2}} \kappa v_\phi O_\chi^{i1} O_+^{j1} O_+^{k2} \tag{B4}
\end{aligned}$$

and the Feynman rule is,



$$= iM_{h_i h_j^+ h_k^-}.$$


$$= iM_{h_i \Delta^{++} \Delta^{--}}.$$

For one CP -even and two doubly charged Higgs bosons, the relevant term in the Lagrangian is

$$\mathcal{L}_{h_i \Delta^{++} \Delta^{--}} = M_{h_i \Delta^{++} \Delta^{--}} h_i \Delta^{++*} \Delta^{--}, \tag{B5}$$

with

$$M_{h_i \Delta^{++} \Delta^{--}} = -2\lambda_2 v_\Delta O_\chi^{i3} - \lambda_3 v_\phi O_\chi^{i2} - \beta_3 v_\sigma O_\chi^{i1}, \tag{B6}$$

leading to the following Feynman rule

For three CP -even Higgs bosons, the relevant term in the Lagrangian is

$$\mathcal{L}_{h_i h_j h_k} = M_{h_i h_j h_k} h_i h_j h_k, \tag{B7}$$

where we sum over i, j, k . The coupling $M_{h_i h_j h_k}$ (with units of mass), after symmetrization in j and k , is given by

$$\begin{aligned}
M_{h_i h_j h_k} = & -6\lambda_1 v_\phi O_\chi^{i2} O_\chi^{j2} O_\chi^{k2} - 6(\lambda_2 + \lambda_4) v_\Delta O_\chi^{i3} O_\chi^{j3} O_\chi^{k3} \\
& - (\lambda_3 + \lambda_5) v_\phi \left[O_\chi^{i2} O_\chi^{j3} O_\chi^{k3} + O_\chi^{k2} O_\chi^{i3} O_\chi^{j3} + O_\chi^{j2} O_\chi^{k3} O_\chi^{i3} \right] \\
& - [(\lambda_3 + \lambda_5) v_\Delta - \kappa v_\sigma] \left[O_\chi^{i2} O_\chi^{j2} O_\chi^{k3} + O_\chi^{k2} O_\chi^{i2} O_\chi^{j3} + O_\chi^{j2} O_\chi^{k2} O_\chi^{i3} \right] - 6\beta_1 v_\sigma O_\chi^{i1} O_\chi^{j1} O_\chi^{k1} \\
& - \beta_2 v_\phi \left[O_\chi^{i1} O_\chi^{j1} O_\chi^{k2} + O_\chi^{k1} O_\chi^{i1} O_\chi^{j2} + O_\chi^{j1} O_\chi^{k1} O_\chi^{i2} \right] \\
& - (\beta_2 v_\sigma - \kappa v_\Delta) \left[O_\chi^{i1} O_\chi^{j2} O_\chi^{k2} + O_\chi^{k1} O_\chi^{i2} O_\chi^{j2} + O_\chi^{j1} O_\chi^{k2} O_\chi^{i2} \right] \\
& - \beta_3 v_\Delta \left[O_\chi^{i1} O_\chi^{j1} O_\chi^{k3} + O_\chi^{k1} O_\chi^{i1} O_\chi^{j3} + O_\chi^{j1} O_\chi^{k1} O_\chi^{i3} \right] \\
& - \beta_3 v_\sigma \left[O_\chi^{i1} O_\chi^{j3} O_\chi^{k3} + O_\chi^{k1} O_\chi^{i3} O_\chi^{j3} + O_\chi^{j1} O_\chi^{k3} O_\chi^{i3} \right] \\
& + \kappa v_\phi \left[O_\chi^{i1} O_\chi^{j2} O_\chi^{k3} + O_\chi^{i1} O_\chi^{k2} O_\chi^{j3} + O_\chi^{j1} O_\chi^{i2} O_\chi^{k3} + O_\chi^{k1} O_\chi^{i2} O_\chi^{j3} + O_\chi^{j1} O_\chi^{k2} O_\chi^{i3} + O_\chi^{k1} O_\chi^{j2} O_\chi^{i3} \right] \quad (B8)
\end{aligned}$$

The corresponding Feynman rule is given by

$$= iM_{h_2 h_1 h_1}.$$

-
- [1] G. Aad *et al.* (ATLAS), Phys. Lett. **B716**, 1 (2012), arXiv:1207.7214 [hep-ex].
- [2] S. Chatrchyan *et al.* (CMS), Phys. Lett. **B716**, 30 (2012), arXiv:1207.7235 [hep-ex].
- [3] J. W. F. Valle, Prog. Part. Nucl. Phys. **26**, 91 (1991).
- [4] J. Schechter and J. W. F. Valle, Phys. Rev. **D25**, 774 (1982).
- [5] The connexion between the neutrino sector of the model and collider physics arises via the decays of the doubly charged Higgs (arising from the triplet) to charged leptons, as these decays involve the same Yukawas above mentioned.
- [6] J. Schechter and J. W. F. Valle, Phys. Rev. **D22**, 2227 (1980).
- [7] E. Accomando *et al.*, (2006), 10.5170/CERN-2006-009, arXiv:hep-ph/0608079 [hep-ph].
- [8] E. J. Chun, K. Y. Lee, and S. C. Park, Phys. Lett. **B566**, 142 (2003), arXiv:hep-ph/0304069 [hep-ph].
- [9] H. Nishiura and T. Fukuyama, (2009), arXiv:0909.0595 [hep-ph]; A. G. Akeroyd, M. Aoki, and H. Sugiyama, Phys. Rev. **D77**, 075010 (2008), arXiv:0712.4019 [hep-ph]; J. Garayoa and T. Schwetz, JHEP **03**, 009 (2008), arXiv:0712.1453 [hep-ph]; P. S. Bhupal Dev, D. K. Ghosh, N. Okada, and I. Saha, JHEP **03**, 150 (2013), [Erratum: JHEP05,049(2013)], arXiv:1301.3453 [hep-ph].
- [10] T. P. Cheng and L.-F. Li, Phys. Rev. **D22**, 2860 (1980).
- [11] M. A. Diaz, M. A. Garcia-Jareno, D. A. Restrepo, and J. W. F. Valle, Nucl. Phys. **B527**, 44 (1998), arXiv:hep-ph/9803362 [hep-ph].
- [12] A. G. Akeroyd, M. A. Diaz, M. A. Rivera, and D. Romero, Phys. Rev. **D83**, 095003 (2011), arXiv:1010.1160 [hep-ph].
- [13] G. B. Gelmini and M. Roncadelli, Phys. Lett. **B99**, 411 (1981).
- [14] C.-W. Chiang, T. Nomura, and K. Tsumura, Phys. Rev. **D85**, 095023 (2012), arXiv:1202.2014 [hep-ph]; A. G. Akeroyd and S. Moretti, Phys. Rev. **D84**, 035028 (2011), arXiv:1106.3427 [hep-ph]; A. G. Akeroyd and H. Sugiyama, Phys. Rev. **D84**, 035010 (2011), arXiv:1105.2209 [hep-ph]; A. G. Akeroyd, C.-W. Chiang, and N. Gaur, JHEP **11**, 005 (2010), arXiv:1009.2780 [hep-ph]; A. G. Akeroyd and C.-W. Chiang, Phys. Rev. **D80**, 113010 (2009), arXiv:0909.4419 [hep-ph]; P. Fileviez Perez, T. Han, G.-y. Huang, T. Li, and K. Wang, Phys. Rev. **D78**, 015018 (2008), arXiv:0805.3536 [hep-ph]; A. G. Akeroyd and M. Aoki, Phys. Rev. **D72**, 035011 (2005), arXiv:hep-ph/0506176 [hep-ph].
- [15] J.-F. Shen, Y.-P. Bi, Y. Yu, and Y.-J. Zhang, Int. J. Mod. Phys. **A30**, 1550096 (2015); J. Cao, Y.-H. Gao, and J.-F. Shen, Europhys. Lett. **108**, 31003 (2014); J. F. Shen and J. Cao, J. Phys. **G41**, 105003 (2014); J. Cao and J.-F. Shen, Mod. Phys. Lett. **A29**, 1450092 (2014); K. Yagyu, *International Workshop on Future Linear Colliders (LCWS13) Tokyo, Japan, November 11-15,*

- 2013, (2014), arXiv:1405.5149 [hep-ph].
- [16] Y. Yu, Y.-P. Bi, and J.-F. Shen, Phys. Lett. **B759**, 513 (2016); C.-W. Chiang, S. Kanemura, and K. Yagyu, Phys. Rev. **D93**, 055002 (2016), arXiv:1510.06297 [hep-ph]; K.-m. Cheung, R. J. N. Phillips, and A. Pilaftsis, Phys. Rev. **D51**, 4731 (1995), arXiv:hep-ph/9411333 [hep-ph]; R. Godbole, B. Mukhopadhyaya, and M. Nowakowski, Phys. Lett. **B352**, 388 (1995), arXiv:hep-ph/9411324 [hep-ph].
- [17] G. Barenboim, K. Huitu, J. Maalampi, and M. Raidal, Phys. Lett. **B394**, 132 (1997), arXiv:hep-ph/9611362 [hep-ph].
- [18] F. Arbabifar, S. Bahrami, and M. Frank, Phys. Rev. **D87**, 015020 (2013), arXiv:1211.6797 [hep-ph].
- [19] A. G. Akeroyd, S. Moretti, and H. Sugiyama, Phys. Rev. **D85**, 055026 (2012), arXiv:1201.5047 [hep-ph]; A. G. Akeroyd and C.-W. Chiang, Phys. Rev. **D81**, 115007 (2010), arXiv:1003.3724 [hep-ph].
- [20] Y.-J. Zhang, J. Cao, and W.-Q. Zhang, Int. J. Theor. Phys. **55**, 3981 (2016).
- [21] J.-F. Shen, Y.-P. Bi, and Z.-X. Li, Europhys. Lett. **112**, 31002 (2015).
- [22] G. Aad *et al.* (ATLAS, CMS), *Proceedings, Meeting of the APS Division of Particles and Fields (DPF 2015): Ann Arbor, Michigan, USA, 4-8 Aug 2015*, Phys. Rev. Lett. **114**, 191803 (2015), arXiv:1503.07589 [hep-ex].
- [23] K. A. Olive *et al.* (Particle Data Group), Chin. Phys. **C38**, 090001 (2014).
- [24] M. Carena, A. de Gouvea, A. Freitas, and M. Schmitt, Phys. Rev. **D68**, 113007 (2003), arXiv:hep-ph/0308053 [hep-ph].
- [25] E. K. Akhmedov, Z. G. Berezhiani, R. N. Mohapatra, and G. Senjanovic, Phys. Lett. **B299**, 90 (1993), arXiv:hep-ph/9209285 [hep-ph].
- [26] V. Berezhinsky and J. W. F. Valle, Phys. Lett. **B318**, 360 (1993), arXiv:hep-ph/9309214 [hep-ph]; M. Lattanzi, AIP Conf. Proc. **966**, 163 (2007), arXiv:0802.3155 [astro-ph].
- [27] A. Falkowski, F. Riva, and A. Urbano, JHEP **11**, 111 (2013), arXiv:1303.1812 [hep-ph].
- [28] A. Alloul, N. D. Christensen, C. Degrande, C. Duhr, and B. Fuks, Comput. Phys. Commun. **185**, 2250 (2014), arXiv:1310.1921 [hep-ph].
- [29] J. Alwall, R. Frederix, S. Frixione, V. Hirschi, F. Maltoni, O. Mattelaer, H. S. Shao, T. Stelzer, P. Torrielli, and M. Zaro, JHEP **07**, 079 (2014), arXiv:1405.0301 [hep-ph].
- [30] P. Vankov, *Proceedings, Symposium on Hadron Collider Physics Symposium 2011 (HCP 2011): Paris, France, November 14-18, 2011*, EPJ Web Conf. **28**, 12069 (2012), arXiv:1201.5469 [physics.ins-det]; *Proceedings, Community Summer Study 2013: Snowmass on the Mississippi (CSS2013): Minneapolis, MN, USA, July 29-August 6, 2013*, (2013), arXiv:1307.7135 [hep-ex].
- [31] M. Bicer *et al.* (TLEP Design Study Working Group), *Proceedings, Community Summer Study 2013: Snowmass on the Mississippi (CSS2013): Minneapolis, MN, USA, July 29-August 6, 2013*, JHEP **01**, 164 (2014), arXiv:1308.6176 [hep-ex].
- [32] H. Baer, T. Barklow, K. Fujii, Y. Gao, A. Hoang, S. Kanemura, J. List, H. E. Logan, A. Nomerotski, M. Perelstein, *et al.*, (2013), arXiv:1306.6352 [hep-ph].
- [33] H. Abramowicz *et al.* (CLIC Detector and Physics Study), *Proceedings, Community Summer Study 2013: Snowmass on the Mississippi (CSS2013): Minneapolis, MN, USA, July 29-August 6, 2013*, (2013), arXiv:1307.5288 [hep-ex].
- [34] J. F. Gunion, H. E. Haber, G. L. Kane, and S. Dawson, Front. Phys. **80**, 1 (2000).
- [35] M. Carena, I. Low, and C. E. M. Wagner, JHEP **08**, 060 (2012), arXiv:1206.1082 [hep-ph].
- [36] F. del Aguila and J. A. Aguilar-Saavedra, Nucl. Phys. **B813**, 22 (2009), arXiv:0808.2468 [hep-ph].
- [37] F. de Campos, O. J. P. Eboli, J. Rosiek, and J. W. F. Valle, Phys. Rev. **D55**, 1316 (1997), arXiv:hep-ph/9601269 [hep-ph].
- [38] S. Moretti, Eur. Phys. J. **C34**, 157 (2004), arXiv:hep-ph/0306297 [hep-ph].
- [39] S. Komamiya, Phys. Rev. **D38**, 2158 (1988).